INCORPORATING STIMULI-RESPONSIVE DNA STRANDS WITH FUNCTIONAL NANOMATERIAL FOR BIOPHYSICAL AND ANALYTICAL APPLICATIONS

By

YUNFEI ZHANG

A THESIS PRESENTED TO THE GRADUATE SCHOOL
OF THE UNIVERSITY OF FLORIDA IN PARTIAL FULFILLMENT
OF THE REQUIREMENTS FOR THE DEGREE OF
MASTER OF SCIENCE

UNIVERSITY OF FLORIDA

2011

To my beloved parents and fiancé

ACKNOWLEDGMENTS

First, I wish to express my sincerest gratitude to my exceptional research advisor, Dr. Weihong Tan, for offering me such a precious opportunity to study and research under his guidance during the two year studies at University of Florida. His precious advice, inspiration and encouragement strongly encourage me to be a more confident person and a better scientist. I also appreciate his unselfish supporting to me fighting against all the difficulties I faced in this two years, which will definitely have a great impact throughout my life and career.

I would also like to express my sincere thanks to my committee members, Dr. David Powell, and Dr. Nicolo Omenetto for the helpful discussion, advice and assistance. I really want to thank Dr. Nicolo Omenetto for his guidance in course study and thank Dr. Powell for his kindest help in my first year MS study. I also want to thank Dr. Ben Smith for all the help and support in this two years. In particular, I would also like to thank Dr. Kathryn R. Williams for her kindness and help with the experiments and manuscripts.

This thesis is a result of successful collaboration with many great scientists in different areas. I especially would like to thank Dr. Quan Yuan for the guidance, tremendous help and friendship during me first two years of research. I want to greatly thank Dr. Yan Chen for all her guidance in my research and help in my personal help. I want to thank Meghan B. O'Donoghue for her patient guidance to teach me and help me in all the cell experiment. I am grateful to Mingxu You for the many helpful discussions on different projects as a knowledgeable friend. I am thankful to Dr. Zhi Zhu for being there whenever I need any help or advice. I thank Dr. Huaizhi Kang for her

help in Azobenzene DNA synthesis and purification. Also I would like to thank Tao Chen for all the helpful discussions.

It has been a great time and experience in the Tan research group, and it is my great pleasure to meet so many kind and nice friends here. I would like to thank Dr. Kwame Sefah, Dr. Kelong Wang, Dr. Ling Meng, Dalia Lopez Colon, Hui Wang, Suwussa Bamrungsap, Xiangling Xiong, Basri Gulbakan, Lu Peng, Da Han, Guizhi Zhu Emir Yasun, Ismail öçsoy, and others for their friendship and help. Each of them has made the time very enjoyable and pleasant.

Also, I am deeply grateful to my fiancé, He Wei, for his selfless supporting to all my important choice in my life. I appreciate all the things he has dedicated for our love, and for our future. His smile is the strongest motivation in my life.

Finally, I owe a huge debt of gratitude to my parents, for their sincerest love, encouragement, and support to me. Their endless love and constant guidance make me who I am. I really appreciate their unselfish dedication to me all this time. I also want to thank my four-years-old younger sister; she is the most beautiful sunshine in my life, forever and ever.

TABLE OF CONTENTS

page

LIST OF TABLES

LIST OF FIGURES

Abstract of Thesis Presented to the Graduate School
of the University of Florida in Partial Fulfillment of the
Requirements for the Degree of Master of Science

INCORPORATING STIMULI-RESPONSIVE DNA STRANDS WITH FUNCTIONAL NANOMATERIAL FOR BIOPHYSICAL AND ANALYTICAL APPLICATIONS

By

Yunfei Zhang

August 2011

Chair: Weihong Tan
Major: Chemistry

Due to their functionality, stability, versatility, and programmability, nucleic acids have received extensive attention in the scientific community as outstanding nanoscale macromolecule materials [1]. Several external stimuli such as light irradiation fluctuation, ion concentration variation, temperature change, electric field oscillation, and pH change can cause the geometry or formation change. Through the specific and rapid response to external stimuli, it is promising to design nucleic acids that serve into molecular sensors and nanoscale molecular motors. On the other side, the nanoscale sizes endow particles with interesting properties, including the surface-plasmon resonances of noble metal nanoparticles, and the porous structure of mesoporous silica nanoparticles. My research projects focus on combining both the advantages of stimuli-responsive DNA and the optical and structural properties of nanoparticles, in order to realize the development of high efficiency DNA nanomotor, DNA controlled release system, and DNA-based ion detection in different systems.

The first project was to use silver nanoparticle for developing highly efficient light-driven azobenzene incorporated DNA nanomachine. Various DNA-based nanomotor

have been investigated due to the fast development of DNA technology. For instance, Light-driven DNA motor with good reversibility has shown its great potential in converting photonic energy into kinetic energy of molecular scale movement; however, the challenge of nanomotor is set by its low conversion efficiency. We developed here a silver nanoparticle enhanced DNA nanomotor system, which significantly improved working efficiency of DNA motors than previous works. The enhancement mechanism was proposed through surface-plasmon resonance effect, which was simulated and explained by the theoretical calculation of surface plasmonic localized electric field distribution. The early success makes us believe this work could potentially benefit the future development of more efficient light-driven DNA nanomotor.

The second project employed the light-driven azo-DNA to devise a light-controlled release system based on mesoporous materials. Light control has the advantages of simple operation, rapid response, and high reversibility. With large inner space and homogeneous porous structure, mesoporous silica nanoparticles have functioned as good cargo carriers. Through capping the pores of mesoporous nanoparticle with azo-DNA strands, cargo release could be controlled by different light irradiations. By switching the irradiation wavelength (365nm for releasing, 450nm for capping), a fast-response, highly-reversible controlled release system has been designed and fabricated, possibly contributing to the controllable drug release in therapeutic medicine and pharmacology.

The third project was the conjugation of Hg^{2+} sensitive T-rich DNA to mesoporous silica nanoparticles for sensitively detecting Hg^{2+} through a signal-amplification process. As is well-known, mercury pollution is a serious problem posing severe health risks to

humans even at very low concentrations. Traditional detection methods usually require complicated sample preparation and expensive instruments, and it is therefore imperative to develop an easy and simple detection approach for Hg^{2+} detection. In this project, mesoporous silica nanoparticles acted as a dye carrier and were capped by T-rich DNA. In the presence of Hg^{2+},T-rich DNA with a stronger binding with Hg^{2+} detached from the nanoparticle, followed by the release of the dye cargo, and thus the detection of Hg^{2+} was realized by measuring the fluorescence intensity of the released dye. This approach was approved to have the lowest detection limit down to ppb level. The detection could be achieved in a short time and without any interference from other metal ions. The great potentials of this Hg^{2+} sensing system would be further tested for detecting aqueous contamination in real sample.

In summary, my research has mainly focused on the molecular design of DNA strands functionalized nanoparticles for guest molecule delivery, ion detection, and nanomotor development. I expect to explore more in the biomedical area in the future.

CHAPTER 1
BACKGROUND

Review of Nucleric Acid

Discovery of Nucleic Acids

Nucleic acids are biological molecules that contain most of human's genetic information. They were first discovered by Friedrich Miescher from the nuclei of white blood cells in 1869 in Felix Hoppe-Seyler's laboratory at the University of Tübingen, Germany[2]. The double helix structure of nucleic acid was pioneering elucidated in 1953 by Watson and Crick[3].

Composition and Structure of Nucleic Acids

Generally nucleic acids can be divided into two main groups: deoxyribonucleic acid(DNA) and ribonucleic acid(RNA) according to their difference in the formation of nucleotides. Nucleotides are building blocks of nucleic acids macromolecule, and each nucleotide can be divided into three components: a nucleobase, a pentose sugar and a phosphate group. DNA and RNA are just distinguished by a hydroxyl group in sugar. DNA has 2'-deoxyribose while RNA has ribose. The nucleobase can be also labeled into two groups: the purines group, labeled as adenine(A) and guanine(G), the pyrimidines group, labeled as cytosine(C), uracil(U) and thymine(T) (structures shown in Figure 1-1, thymine only exists in DNA and uracil only exists in RNA). The nucleotides are connected by phosphodiester linkages between sugars and phosphates to form a sugar-phosphate backbone(Shown in Figure1-2) and the ends of each nucleic acid chain are labeled as 3' and 5'. The nucleobases have covalent binding to the sugar-phosphate backbone via an N-glycosidic linkage between a nucleobase ring nitrogen and a carbon on the pentose sugar ring.

The Principle of Complementary Base Pairing

A significant important discovery was reported by Chargaff et al[4]. A double-stranded DNA molecule has percentage base pair equality between adenine(A) and thymine(T), guanine(G) and cytosine(C), although base compositions are valid for each of the two DNA strands. Afterwards the famous Watson-Crick double helix DNA structure was proposed, in which the double strands DNA are formed by hydrogen bonding between purine and pyrimidine. In the typical Watson-Crick DNA base pairing, adenine (A) forms two hydrogen bonding with thymine (T) and guanine (G) forms three hydrogen bonding with cytosine (C)(as shown in Figure 1-3). Additionally, thymine is replaced by uracil (U) in RNA. In this helix structure of DNA duplex the nucleotides are paired in the middle while the ribose sugar and phosphate groups that form the backbone are exposed at outer edge. Generally DNA molecules are mostly double-stranded in contrast RNA molecules are mostly single-stranded, but the exceptions also exist.

Stimuli-response DNA Switches

A single strand DNA molecule has a strong potential of recognizing and hybridizing with its complementary sequence through this highly specific complimentary base-pairing interactions. This remarkable specificity enables DNA strands coupled other functional moieties to form the specific nanostructures or nanomachine which undergo structural transitions in response to external stimuli. Such stimuli include complimentary strand, pH change, ions, light irradiation, electrical field and temperature change.

PH-responsible DNA switches

The famous pH-responsive DNA structure i-motif, discovered by Gueron *et al.* in 1993, is the C-rich DNA strand which switches between “cubic” and “linear” structure by base-pairing between short stretches of protonated and unprotonated cytosines[5]. The protonated cytosine can form a self-hybridized structure with three hydrogen bonding(shown in Figure 1-4 A)**.** Gueron designed a DNA strand 5’-d(TCCCCC) and found it formed a “quadruplex” structure in the acidic surrounding ,while in basic surrounding this structure would be destroy and return back to the initially linear structure. This pH-responsive DNA switching has been widely used as a pH sensor or pH driven nanomotor. Liu and Balasubramanian *et al.*have developed an i-motif based pH DNA sensor by labeling the ends of i-motif with fluorophore and quencher[6]. At acidic pH i-motif strand folded into the closed i-motif structure then fluorophore was quenched, while at basic pH i-motif strands returned to linear state and the fluorescence expressed again. Shu *et al.* developed an i-motif based DNA motor based motivated by pH switching[7], which converted biochemical reactions into mechanical work through the conformational change of i-motif strands. Chen *et al.* developed a pH-controlled release system by capping pore outlets of mesoporous silica nanoparticles with i-motif DNA strand[8]. The open-close of the pore was controlled by the geometry change of i-motif at different pH and this process was highly reversible. And the pH sensitive DNA can even be utilized to map pH changes in living *Caenorhabditis elegans* worm[9], which suggested a great potential of i-motif DNA strands in *in vivo* pH monitoring.

Light-responsible DNA switches

The light driven DNA strands are usually coupled with photo-sensitive molecules such as azobenzene[10] and 2-nitrobenzyl linker[11]. The synthesis protocol of 2-nitrobenzyl

linker bridging photocleavable DNA was reported by Bai *et al.* in 2002[11]. By introducing 1-nitrobenzyl linker into DNA strands, the DNA molecule can be efficiently and rapidly cleaved under UV irradiation. In 2007 Asanuma *et al.* reported a detailed protocol for the synthesis of azobenzene phorsphoramidite tethered to DNA to make it photoresponsive[10]. Azobenzene is a photo-responsive molecule that isomerizes between its planar *trans*-form and non-planar *cis*-form under different light irradiation. Tethered with azobenzene molecule, the hybridization of DNA duplex can be controlled by switching the irradiation source. Light-driven DNA nanomotor structure were under this mechanism[12]. The nanomotor was completely reversible, and did not decompose or induce undesirable side reactions after repeated more than 10 cycles. Also a light controlled DNA 3 dimensional structure was discovered, where the geometry of a DNA tetrahedron was controlled by switching light irradiations of different wavelengths[13].

Ion-responsible DNA switches

Besides the principle of complementary base A-T AND C-G pairing roles, DNA nucleobases have some abnormal pairings with the existence of metal ions such as Hg^{2+} and Ag^{+}. Hg^{2+} can selectively bind to two thymine (T) bases and forms stable Thymine-Hg^{2+}- Thymine complexes, which are even more stable than the T-A Watson-Crick matching(shown in Figure 1-4 B). And additionally, this interaction is highly specific as only Hg^{2+} can form the Thymine-Thymine mismatching base pair. Ag^{+} has a similar property but associate with two cytosine forming Cytosine-Ag^{+}-Cytosine complexes (shown in Figure 1-4 C). This specific interaction between metal cation and DNA has been thoroughly used in the design of molecular beacon for the ion detection. Lin *et al.* developed a colorimetric approach using DNA-functionalized gold nanoparticles for the detection of mercuric ion[14]. This approach took advantage of both

catalytic properties of DNA-functionalized gold nanoparticles and the specific binding of a Cytosine- Ag^+-Cytosine mismatch, and consequently it realized selectively detection of Ag^+ from 19 other metal ions. Lin *et al.* reported an inexpensive method, where DNA-functionalized hydrogel system for ultrasensitive detection and removal of Hg^{2+} in water [15]. In these works DNA strands always give a rapid and sensitive response to the target metal ions, suggesting a brightly future of using ion stimuli-responsive DNA for the ultrasensitive, instrument-free, rapid and visual detection of metal ions.

The Surface Plasma Resonance of Metal nanoparticles

Nanoscale metal particle has the unique optical property of surface-plasmon resonances, which are quantized electron oscillations that confined to nanoscale volumes. The first theory of light scattering and absorption by gold nanosphere was reported by Gustav Mie more than a hundred years ago[16] and several modern theories have been developed after that. While metals or semiconductors is irradiated by visible electromagnetic waves, the collective oscillation of conduction band electrons will occur and the electron excitations is defined as *Plasmons*[17]. On bulk metal or extended metal surface, plasmons are free to propagate, while on a nanoscale metal particle plasmons are imposed with a boundary condition to a finite volume. From Mie theory, the extinction cross-section C_{ext}, for the scattering of a metal nanosphere can be calculated by equation:

$$C_{ext}(\omega,R)=12\pi\frac{\omega R^3\varepsilon_m^{3/2}}{c}\frac{\varepsilon_2(\omega,R)}{[\varepsilon_1(\omega,R)+2\varepsilon_m]^2+\varepsilon_1(\omega,R)^2} \quad (17)$$

In this equation R is the radius of nanosphere, c is the speed of light, ε_m is the frequency-independent dielectric constant of the medium (ω is the frequency) and ε(ω,

R) = $\varepsilon_1(\omega, R) + i\varepsilon_2(\omega, R)$, while ε1(ω, R) and $i\varepsilon_2(\omega, R)$ are the real and complex parts of the material dielectric constant. Plasmons spherical particles are dipolar which results in only a single plasmon resonance peak, while the anisotropic nanoparticles such as nanorod and nanoprism can support many plasmon modes[18]. Several methods are applied to get a deeper understanding of the relationship between geometry and optical properties on nanoparticle. Discrete dipole approximation (DDA), is the most widely numerical tool for investigating shape effects on nanoparticle plasmonic in which particle is discretized into elementary subunits that are modeled as dipoles.

From all this equation and principle the optical properties of plasmonic atoms of metal nanoparticle are decided by size and morphology of the particle, material composition and surrounding dielectric environment[19-21], while the size and morphology are the dominating facts. So controlling the size and morphology of metal nanoparticles in synthesis step is the best way to engineer the position and strength of plasmonic resonance bands.

Bio-functionalized Mesoporous Silica Nanoparticles and their Applications

Mesoporous material is the homogeneous material defined by pores diameters between 2 and 50 nm (by IUPAC). The most commonly used mesoporous materials are silica and alumina while other mesoporous oxides as niobium, tantalum, titanium, zirconium, cerium and tin have also been reported. In 1992 a homogeneous mesoporous silica nanosphere was synthesized in Mobil Research and Development Corporation Central Research Laboratory and named as Mobil Crystalline Materials(known as the famous MCM-41)[22]. In 1998 another fiber shaped mesoporous silica nanoparticle was synthesized by Zhao *et al.* in University of California, Santa Barbara and named as Santa Barbara Amorphous type material(noted as SBA-15)[23].

With the advantages of good biocompatibility, large loading capacity, highly ordered pore structure and adjustable pore size, mesoporous silica nanoparticle has already been widely used as carrier vehicles[8,24]. And more because of the numerous silanol group that on the surface, mesoporous silica nanoparticle can be easily be immobilized with various organic or biological molecules as linkers then link to some large molecule to cap the pore, while those linkers can also be cleaved by some specific stimuli which lead to the uncapping of pore and the release of the cargo[24]. The stimuli are like the “key” while the capping is like the “door”. In the recently published paper mesoporous silica nanoparticle can be capped by various of materials such as DNA[25], protein[26,27], nanoparticle[28,29], polymers[30-33] and can also be uncapped by various of stimulates such as heat[26], magnetic field[30], pH[8,24,29], target molecules[28,34], enzyme[31,33,35] or even light[32].

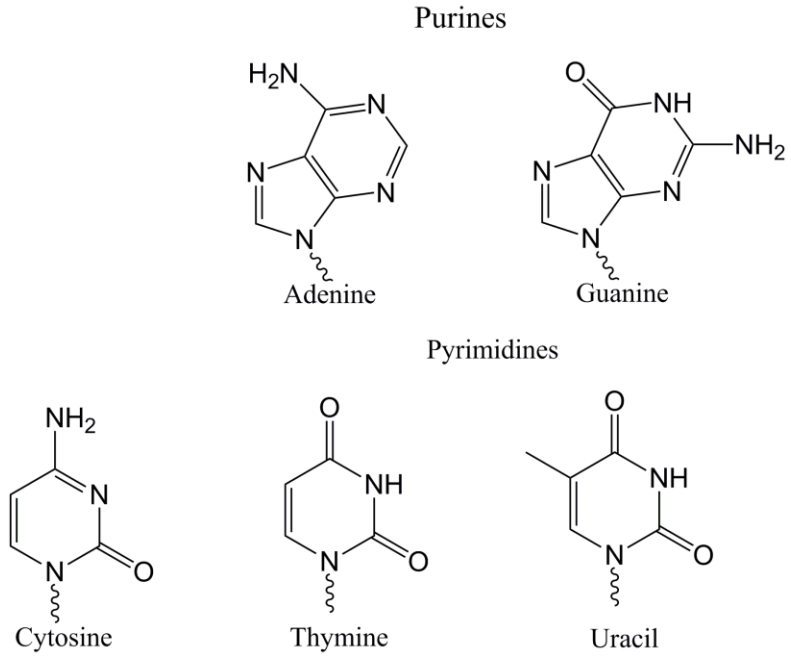

Figure1-1. The general structure of nucleobase

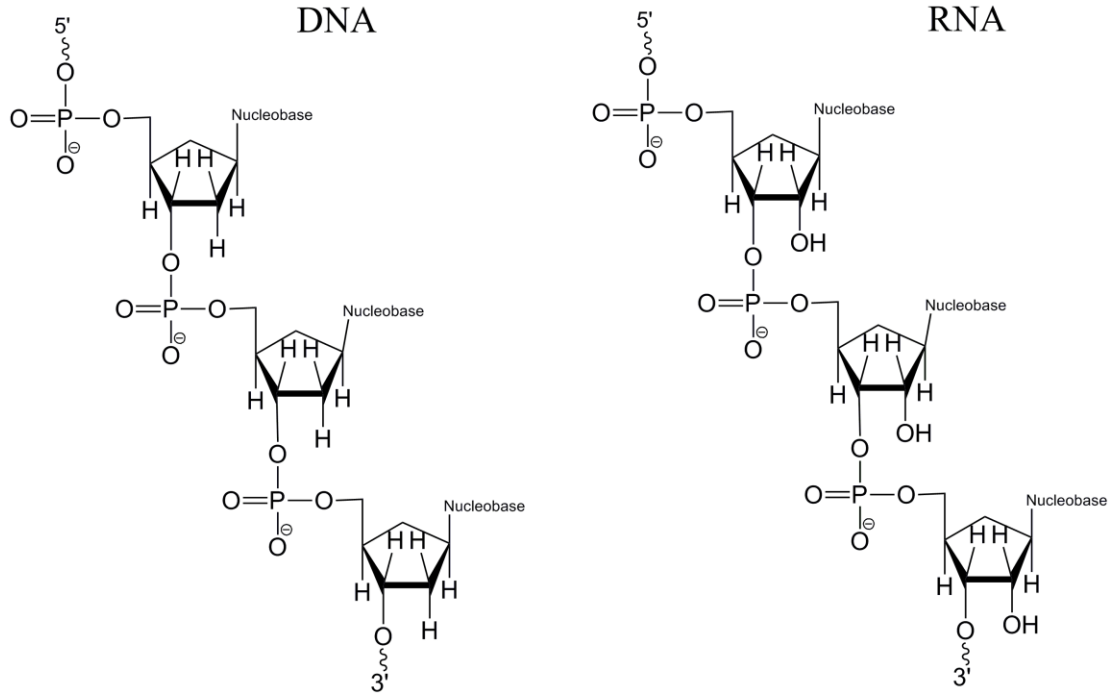

Figure1-2. The backbone structure of DNA and RNA.

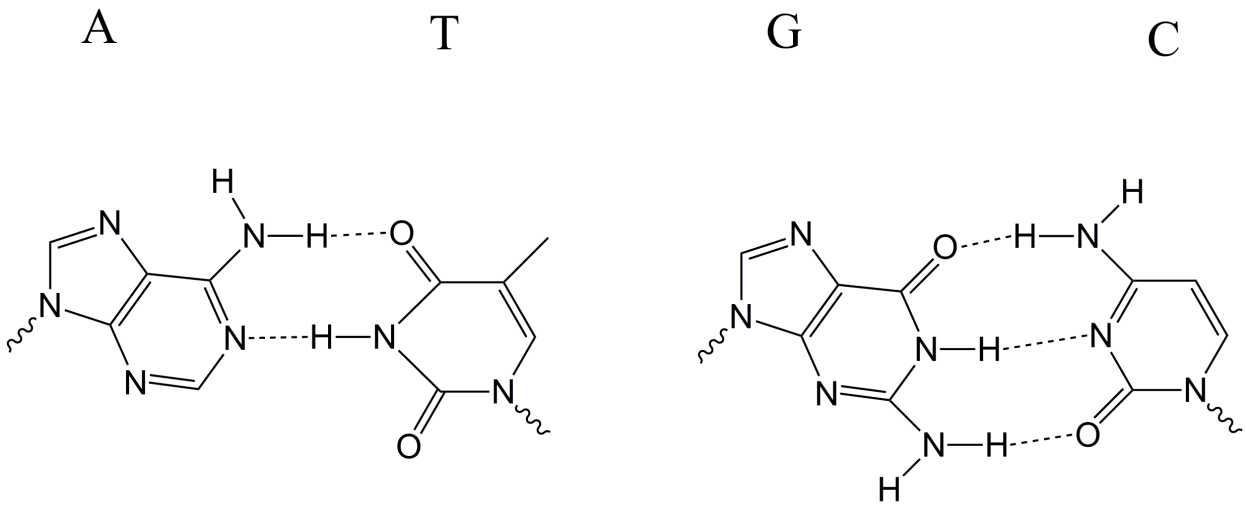

Figure1-3. The principle of complementary base pairing.

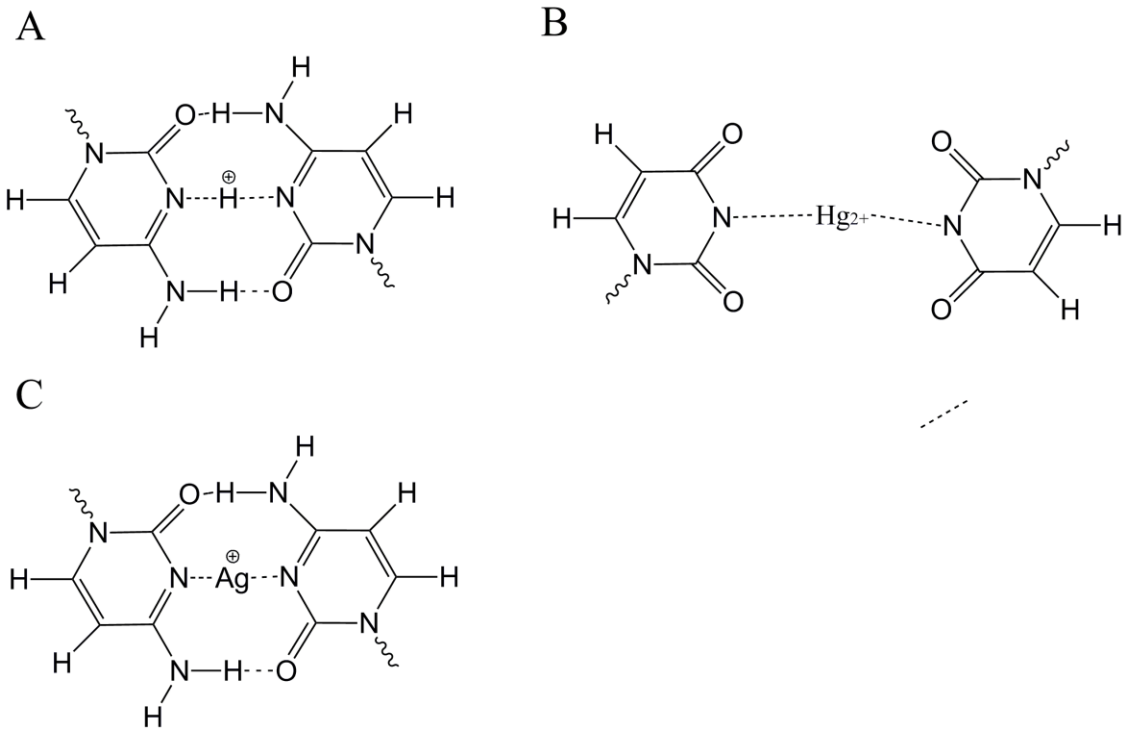

Figure 1-4. The abnormal nucleobase pairings. A) Protonated Cytosine-Cytosine pairing. B) Thymine-Hg^{2+}-Thymine pairing. C) Cytosine-Ag^{+}-Cytosine pairing.

CHAPTER 2
USING SILVER NANOPARTICLE FOR THE ENHANCEMENT OF LIGHT DRIVEN DNA NANOMACHINE

In the recently years, stimuli-responsive DNA has received much attention as nanomachines to make nanoscale movements in response to external stimuli[6,36-39].

In 2009 Kang *et al.* reported a photo-responsive DNA nanomachine with incorporated azobenzene moieties[12], using the photoisomerization of azobenzene to regulate DNA hybridization then control the open and close of DNA Nanomachine. In theoretical calculation the contraction force of a single DNA nanomotor could be in pN level. With the good reversibility of DNA nanomotor, this kind of photo-driven nanomotor promised us a approach to generate photonic energy into mechanical movement. However, the disadvantage of azobenzene DNA nanomotor is the low close-open conversion due to the low photoisomerization efficiency of azobenzene moieties, which is the bottle-neck problem to the further development of light-driven nanodevice applications.

Here, we reported our discovery that silver nanoparticle could enhance the open-close conversion efficiency of DNA nanomotor by plasmonic near-field coupling and spectral overlap with incorporated azobenzene moieties. The open-close conversion efficiency of light-driven DNA nanomotor was enhanced from initial 20% to 85% with the existence of silver nanowire. The experimental results were confirmed by theoretical modeling calculations of the localized electric field distribution and absorbance spectral overlap of silver nanoparticle with different morphology. The DNA nanomotor with enhanced conversion efficiency shows a great potential in light-driven nanomachine design and solar energy conversion.

Experimental Section

Chemicals

All the chemicals to synthesis azobenzene phosphoramidite, Silver and Gold nanoparticle were purchased from Sigma-Aldrich chemical, Inc. The materials for DNA synthesis, including CPG columns and reagents for DNA modification and coupling, were purchased from Glen Research Co.

Instrumentation

The synthesis and coupling of all the DNA sequences were taken out on ABI3400 DNA/RNA synthesizer (Applied Biosystems) .Purifications were carried out on a ProStar HPLC system with a gradient unit(Varian) and a C-18 column(Econosil, 5U, 250X4.6mm)The concentration of DNA sequences were calculated by measuring the absorbance of DNA solution at 260nm on a Cary Bio-300UV spectrometer(Varian). The absorbance spectrum of the entire silver and gold nanoparticle was measured on the same spectrometer. Fluorescence measurements of the DNA motor solution were performed on a Fluorolog-Tau-3 spectrofluorometer (Jobin Yvon).Transmission electron microscopy (TEM) images of all the gold and silver nanoparticle were obtained on a Hitachi H-7000 NAR transmission electron microscope under a working voltage of 100 kV. The fluorescence images were taken by CLSM (IX81, Olympus).

Synthesis of Silver and Gold Nanoparticle

Ag nanosphere

Firstly 2.50 g polyvinylpyrrolidone (PVP M_W = 10,000) was dissolved in 10 mL double distilled water (Millipore, Bioscience Research Reagents), then 3 mL of $AgNO_3$ solution (188 mM) was added. Then the solution was heated at 60 °C for certain time

under stirring (15 min for 6 nm Ag nanosphere and 60 min for 50 nm ones), and then the product was obtained.

Ag nanowire

Ag nanowires were synthesized following a reported method[40]. Firstly 5 mL ethylene glycol was heated to 160 °C and then 0.5 mL 0.12 mM $PtCl_4$ solution (ethylene glycol as solvent) was injected into the solution with magnetic stirring for 4 min. Afterward, 2.5 mL ethylene glycol solution of $AgNO_3$ (20 mg/mL) and 5 mL ethylene glycol solution of poly(vinyl pyrrolidone) (PVP, 40 mg/mL, M_W = 55 000) were simultaneously injected to the ethylene glycol containing platinum seeds. This reaction mixture was stirred at 160 °C 10 min for 1 μm nanowires and 1h for 40 μm ones, respectively. After cooled down to room temperature, the reaction mixture was diluted with acetone (approximate 10 times by volume), and centrifuged at 2000 rpm for 20 min. The nanowire settled down to the bottom of the container under centrifugation while the nanoparticles that still remained in the liquid phase was removed using a pipet. This separation procedure was repeated several times until nanowire samples essentially free of particles were obtained.

Ag nanoprism

25 mL $AgNO_3$ aqueous solution (0.1 mM) was prepared, and then 300 μL of sodium citrate (30 mM), 1.5 mL of PVP (M_w = 29000 g/mol, 3.5 mM), and 60 μL of aqueous H_2O_2 (30 wt %) were added under vigorously stirring at room temperature. Fresh prepared $NaBH_4$ (100 mM, 250 mL) was then rapidly injected into this mixture. Ag triangular nanoplates were obtained after approximately 1 h reaction.

Au nanosphere

Firstly 20 mL $HAuCl_4$ (0.1 mM) solution was heated to boiling under vigorous stirring. Then certain amount of fresh prepared 1 wt% sodium citrate solution (0.40 mL for the 13 nm Au nanospheres and 0.5-0.175 mL for the 50 nm Au nanospheres) was added. The solution was kept boiling until the color turned from dark blue to red. Keep stirring until the solution cool down to the room temperature, then the products were obtained.

Au nanorod

Cetyltrimethylammonium bromide (CTAB) aqueous solution (0.1 M, 10 mL) was mixed with 0.25 mM $HAuCl_4$ (0.25 mL). A freshly prepared, ice-cold 0.01 M $NaBH_4$ (0.6 mL) was added to this solution all at once, followed by rapid inversion mixing for 2 min. The resulting CTAB-stabilized gold nanoparticle seed solution was kept at room temperature for 2 hrs. For seed-mediated growth, $HAuCl_4$ (2 mL, 0.01 M) and $AgNO_3$ (0.4 mL, 0.01 M) were added into CTAB (40 mL, 0.1 M). After gentle mixing of the solution, a freshly prepared ascorbic acid (0.32 mL, 0.1M) was added as a mild reducing agent. Then a portion of the seed solution (0.096 mL) was added. The reaction mixture was mixed by gentle inversion for 10 s and left undisturbed at least overnight to form Au nanorod.

Characterization of Silver and Gold Nanoparticle

The size and morphology of silver and gold nanoparticle were characterized by Transmission electron microscopy (TEM) on a Hitachi H-7000 NAR transmission electron microscope under a working voltage of 100 kV. The high definition image were shown from Figure 2-1(Ag nanoparticle) and Figure 2-2(Au nanoparticle).

Synthesis of Azobenzene Phosphoramidite

Azobenzene phosphoramidite was synthesized according to the protocol reported by Asanuma et al[10](Figure 2-3). Compound 1. 1H NMR ($CDCl^3$): δ 7.96-7.38 (m, 9H), δ 7.12 (d, 1H), δ 4.33 (m, 1H), δ 4.09 (m, 1H), δ 3.98 (d, 2H), δ 1.29 (d, 3H). Compound 2. 1H NMR ($CDCl^3$): δ 8.00-6.78 (m, 23H), δ 4.25 (m, 1H), δ 4.17 (m, 1H), δ 3.77 (s, 6H), δ 3.60 and 3.42 (dd, 2H), 1.23 (d, 3H). Compound 3. 1H NMR ($CDCl^3$): δ 8.00-6.79 (m, 22H), δ 6.62 (d, 1H), δ 4.48 (m, 1H), δ 4.39 (m, 1H), δ 4.21-4.10 (m, 2H), δ 3.77 (s, 6H), δ 3.57-3.34 (m, 4H), δ 2.76-2.72 (m, 2H), δ 1.30-1.25 (m, 15H). 31P (CDCl3): δ 149.

Synthesis and Purification of DNA Sequences

All the DNA sequences used in this project are listed in Table 2-1. Three DNA sequences were all synthesized on ABI 3400 DNA synthesizer. The DNA sequences were loaded and syhthesis protocol was set up according to the operation handbook provided by the synthesizer's manufacturer. Debcyl CPG was used for the synthesis of Azobenzene DNA nanomotor and Normal DNA nanomotor, and the Azobenzene Phosphoramidite was used for the synthesis of Azobenzene DNA nanomotor. All the DNA products were deprotected and cleaved from CPG by incubating with 2mL 1:1 Ammonium hydroxide/ Methylamine for 30min in a 65^{o}C water bath. Afterwhile the supernatant was transferred to a 15mL eppendorf tube and added 250μL 3.0M NaCl and 6.25mL ethanol. The mixture were kept in -20^{o}C until the DNA precipitated. Afterward the mixture was centrifuged at 400 rpm for 30 min. The supernatant solution was removed while the precipitated DNA was redissolved in 400μL trithylamine acetate (TEAA) for the next purification step.

The DNA/TEAA solution was purified in a C18 column on Varian Prostar HPLC machine. The collected DNA solution was dried in a vacuum dryer and then detritylated in 80% acetic acid for 30mins. Then the detritylated DNA was precipitated in 500μL ethanol with 20μL 3M NaCl again. The ethanol supernatant was removed and then the DNA was dissolves in 400μL de-ionized water. The concentration of DNA was calculated by measuring the absorbance of DNA solution, while the extinction coefficient of each sequence was calculated on Integrated DNA Technologies website. The extinction coefficient of the azobenzene moiety was calculated as 4,100 M^{-1}/cm^{-1} [12]. All the DNA products were kept in -20^{o}C freezer, while the azobenzene DNA should avoid all kind of direct light irradiation.

Irradiation Source

In order to test the conversion efficiency of azobenzene DNA nanomotor under irradiations with specific wavelength, two kinds of light sources have been used: a 60W table lamp with a 450 nm filter was used as a visible light source to turn the azobenzene DNA motor transfer from *Trans*- to *Cis*-, which opened the DNA hairpin structure, and a 23W 60Hz UV lamp with the wavelength at 365 nm was used as a UV light source to turn the azobenzene DNA motor transfer from *Cis*- to *Trans*-, which closed the DNA hairpin structure**.**

Theoretical Calculation of Electric Field Distribution around Nanoparticle

The electric field ($|E|^2$) intensity distributions around the different nanostructures were calculated by finite element method (FEM) using the 3D RF model of COMSOL Femlab. The incident light wavelength was settled as 350 nm while the optical constant of the silver and gold was settled as data reported by Johnson et al[41]. perfectly matched

layers were adopted to avoid spurious reflection effects at the simulation zone boundaries.

Results and Discussion

Design of Light-driven Nanomotor

The design of light-driven DNA nanomotor is shown in Figure 2-4. The DNA motor we designed having a stable hairpin structure with a six-base pair stem and a 19-base loop. And additionally, three azobenzenes were incorporated into the pair stem part so the hybridization of the stem part would be controlled by the irradiation sources. A fluorophore (fluorescein isothiocyanate, noted as FAM) and a quencher (4-dimethylaminoazobenzene-4-carboxylic acid, noted as Dabcyl) were labeled on each ends of the DNA strand so the final sequence design of the azobenzene DNA nanomotor was: 5'-FAM-CCT-AGC-TCT-AAA-TCA-CTA-TGG-TCG-C-Azo-GC-Azo-TA-Azo-GG-Dabcyl-3'. As shown in Figure 2-4, when the DNA nanomotor was under the irradiation with wavelength larger than 400nm, such as the visible light, the DNA motor was in the "close" state then the fluorescence resonance energy transfer between FAM and Debcyl would quench the fluorescence. On the other hand, with the irradiation source in the UV range(300nm<λ<400nm), the photoisomerization of azobenzene would lead to the open of DNA motor, no energy transfer between FAM and Debcyl so the fluorescence could be detected. In this project, fluorescent intensity of FAM excited at 488 nm was used to monitor the light-driven close-open movement of the DNA nanomotor.

Calculation of Conversion Efficiency

The fluorescence intensity of DNA nanomotor under visible light irradiation (I_{Blank}) was settled as baseline and the fluorescence intensity of fully open DNA nanomotor

after addition of excess amount of complementary DNA (5'-GGA-TCG-AGA-TTT-AGT-GAT-ACC-AGC-GCG-ATC-C-3′ noted as cDNA)was settled as 100% (I_{cDNA}). The average close-open conversion efficiency (ε) of the DNA nanomotor for each photon-regulation cycle can be evaluated from the following equation

$$\varepsilon = \frac{I_{UV} - I_{Blank}}{I_{cDNA} - I_{Blank}} \times 100\%$$

while I_{UV} is the fluorescence intensity of DNA motor after UV irradiation.

Enhanced Conversion Efficiency with Ag Nanoparticle

The azobenzene DNA nanomotor without any Ag nanoparticle only has 20% conversion efficiency after 5 min UV irradiation (wavelength=350). Only with the existence of Ag nanoparticle, the conversion efficiency could be enhanced due to the localized electric field created by the Ag nanoparticle under light irradiance(Scheme shown in Figure 2-5).

Enhancement of efficiency also depended on the morphology and size of Ag nanoparticle. To find the Ag nanostructure with the maximum enhancement on DNA nanomotor, Ag nanosphere, Ag nanoprisms , and Ag nanowires with different sizes were all investigated. 1 mL of Ag nanoparticle (2 nM) was washed and centrifuged at 4,000 rpm for 20 min. The precipitated nanoparticle was dispersed in 1 mL of deionized water. 100 μL of the azo-DNA nanomotor solution (50 μM) was added into the solution and incubated overnight to get the maximum absorbance on the surface of Ag nanoparticle. Then the mixture was centrifuged and discarded unadsorbed DNA in supernatant, and the precipitate was dispersed in 1 mL of 8 mM Tris buffer. I_{Blank} was the fluorescence intensity of DNA nanomotor solution that measured under visible light,

while I_{UV} was measured after 5mins UV irradiation (operate in dark room). I_{cDNA} was measured after excess amount of cDNA was added to the solution. Conversion efficiency was calculated using the equation described before. From the results Ag nanowire offered the largest enhancement on DNA nanomotor conversion efficiency, while Ag nanoprism almost had no effect (Results shown in Figure 2-6, Figure 2-7).

Reversibility of Ag Nanowire Enhanced DNA Nanomotor

Although Ag nanowire significantly enhanced the conversion efficiency of DNA nanomotor, the reversibility of this high efficiency should be confirmed. The reversibility of DNA nanomotor with Ag nanowire was tested by alternating 5 min of visible irradiation and 5 min of UV irradiation for ten cycles. As shown in Figure 2-8, even after ten cycles there was no obvious decrease in conversion efficiency. These results confirmed that the enhancement effect was constant in this system.

Fluorescence Micrographs of DNA Nanomotor Conversion

The fluorescent images of DNA motor switching were taken on a confocal laser scanning microscope. DNA nanomotor solutions with and without Ag nanowire were both exposed under the same UV irradiation. Fluorescence micrographs of the DNA nanomotor solution were taken every 30 s to monitor the fluorescence change(Figure2-9). From the fluorescence image It is obvious that the DNA nanomotor solution with Ag nanowire showed higher fluorescence intensity than that without Ag nanowire after UV illumination, confirming the results from spectrafluorometer. From the image DNA nanomotor not only had higher conversion efficiency but also had a faster response with Ag nanowire.

Localized Surface Plasmon of Ag Nanoparticle

In the recently research of light driven molecules, the interaction between azobenzene molecules and metal nanoparticle has been reported[42-44]. For the further study of the origin of this Ag nanoparticle enhancement effect, the near-field behavior of Ag nanoparticle was mimicked using finite element method-based commercial software. When excited by electromagnetic field, the conduction electrons of metallic nanostructure would create nonpropagating localized surface plasmon. The silver nanoparticle used in this project (Ag nanosphere, Ag nanowire, Ag nanoprism)all been tested. The calculation results shows that (Figure 2-10) the electric fields around the Ag nanowires, Ag nanoparticles, and Ag nanoprisms are all strongly localized. The Ag nanowire gave the highest enhanced electric field distribution, especially on both ends, while Ag nanosphere shown a homogeneously enhanced electric field around it. Ag nanoprism also gave a localized enhanced electric field.

Absorbance Spectral of Ag Nanoparticle and Azobenzene Molecule

Only with the calculation results of Ag nanoparticle could not give a complete explanation of Ag nanoparticle's different enhancement effect with different morphology. For further study, the extinction spectral of Ag nanoparticle and absorbance spectral of azobenzene were measured.(Figure 2-11) The azobenzene molecule shown two major absorbance peaks. The low-intensity peak at 440 nm was due to the symmetry-forbidden n – π* transition while the high-intensity at 320 nm was due to the symmetry-allowed π – π* transition*.

Ag nanosphere (50 nm) and Ag nanowire (with length of 1 μm) both shown a narrow extinction peak centered at 430 nm, with the Ag nanoprism did not show any peak here. Their extinction peaks overlap the absorption peak of the azobenzene

molecule. The coupling strength was reported strongly dependent on the spectral overlap between the molecular and plasmonic resonances[45]. So coupling between azobenzene and the plasmonic resonance of both Ag nanosphere and nanowire were confirmed, while the Ag nanoprism which only gave a peak located at 820 nm did not overlap with the absorption peak of azobenzene. This calculated result strongly supported experimental results, the localized electric field created from surface plasmonic resonance and spectral overlap were both the main reason for Ag nanowire to give the highest enhanced conversion efficiency of DNA nanomotor while Ag nanoprism did not.

Au nanoparticle and Effects on DNA Nanomotor

In order to further confirm the mechanism that concluded for the Ag nanoparticle enhancement effect on DNA nanomotor conversion efficiency, Au nanosphere and nanorod, were also tested with DNA nanomotor, but none of them shown an enhancement effect on DNA nanomotor's conversion efficiency (shown in Figure 2-12). The calculation results shown that Au nanosphere also gave localized electric field under the same incidence wavelength, but the extinction peak of Au nanoparticles (around 520 nm) had no overlap with azobenzene absorption peak (shown in Figure2-13). Although the surface plasmonic resonance of Au nanoparticle could create a localized electric field, the conversion efficiency cannot be enhanced due to no coupling between Au nanoparticles and DNA nanomotor azobenzene moiety.

Conclusion

In conclusion, we reported the enhancement effect of Ag nanoparticle for the conversion efficiency of light driven DNA nanomotor. For original mechanism, we demonstrated that Ag nanoparticle's enhancement effect were due to their surface

plasmon resonance-induced localized electric field. With the largest localized electric field and extinction spectral overlap with azobenzene, Ag nanowire increased open-close conversion efficiency of DNA nanomotor from 20% to 85%. For Au nanoparticle with similar localized electric field did not have any enhancement effect as the extinction spectral had no coupling with azobenzene molecule's absorbance spectral. This discovery promised a bright future for future development of high-efficiency light driven nanomotor for multiple purposes.

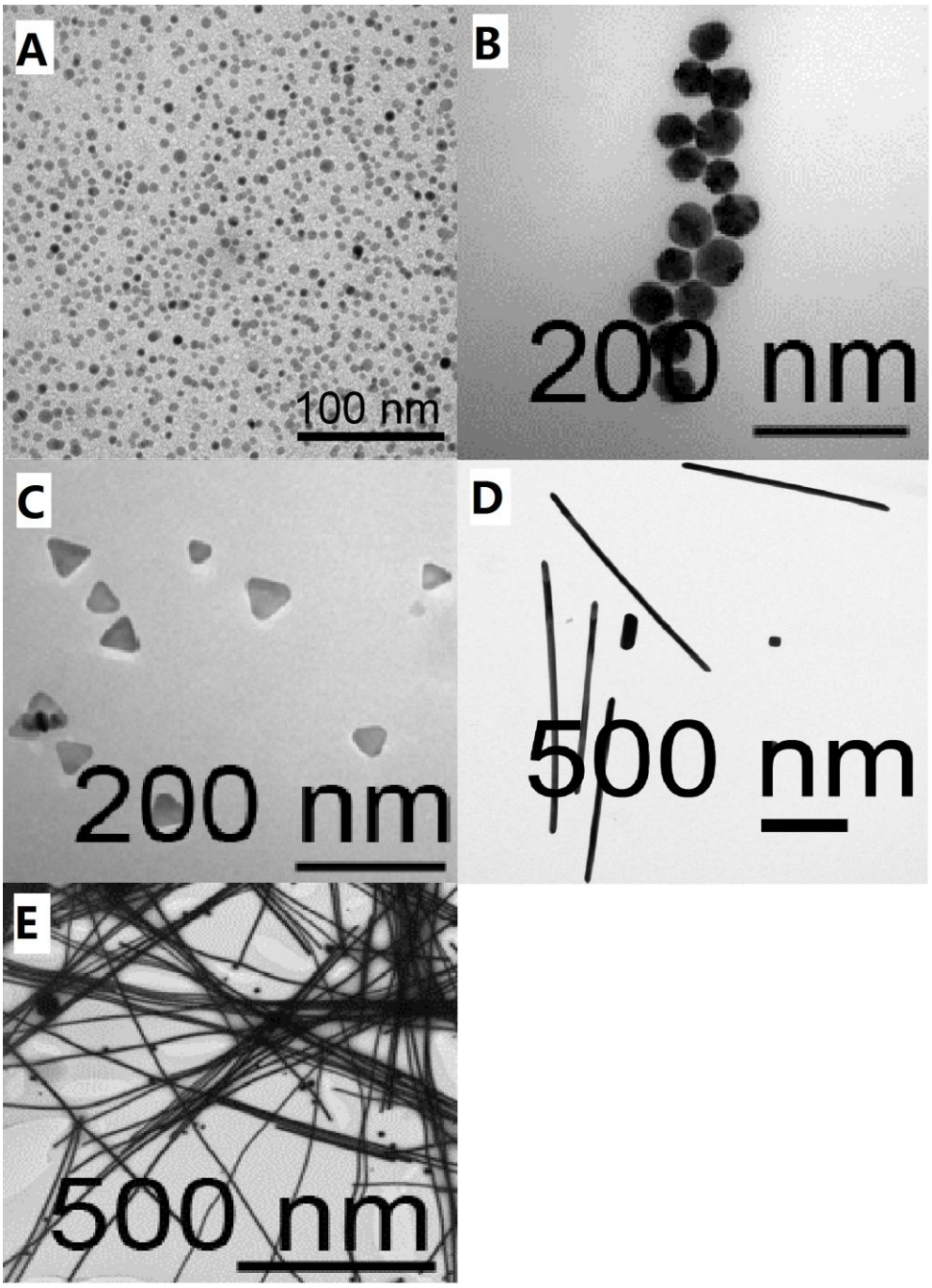

Figure 2-1. Ag nanoparticle with different morphology and size. A) Ag nanosphere (6 nm diameter). B) Ag nanosphere (50 nm diameter). C) Ag nanoprism(50 nm length and 3 nm thickness). D) Ag nanowire (1 μm length). E) Ag nanowire (40 μm length)[46].

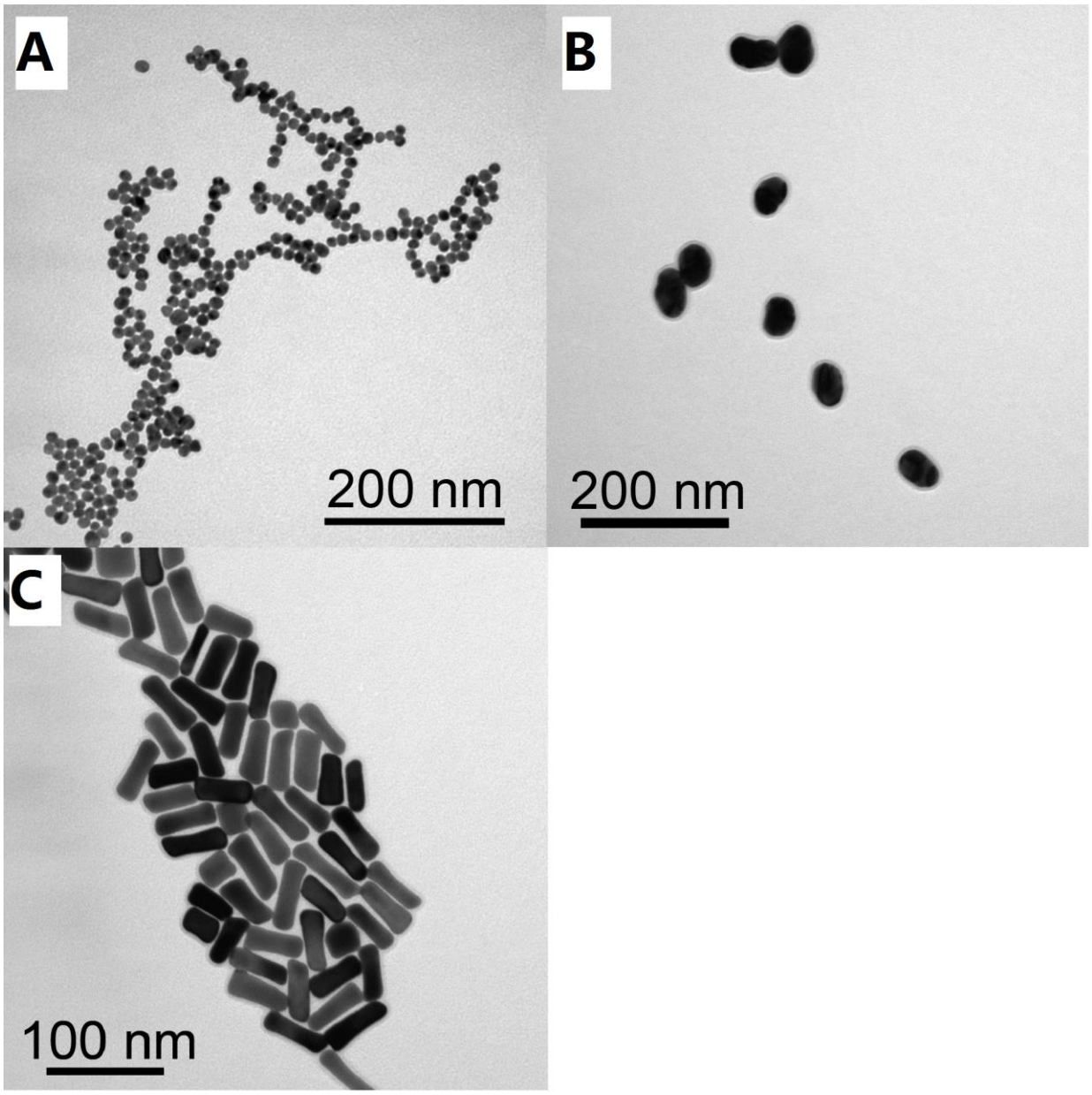

Figure 2-2. Au nanoparticle with different morphology and size. A) Au nanosphere (13 nm diameter). B) Au nanosphere (50 nm diameter). C) Au nanorod (average length of 60nm and width of 13 nm)[46].

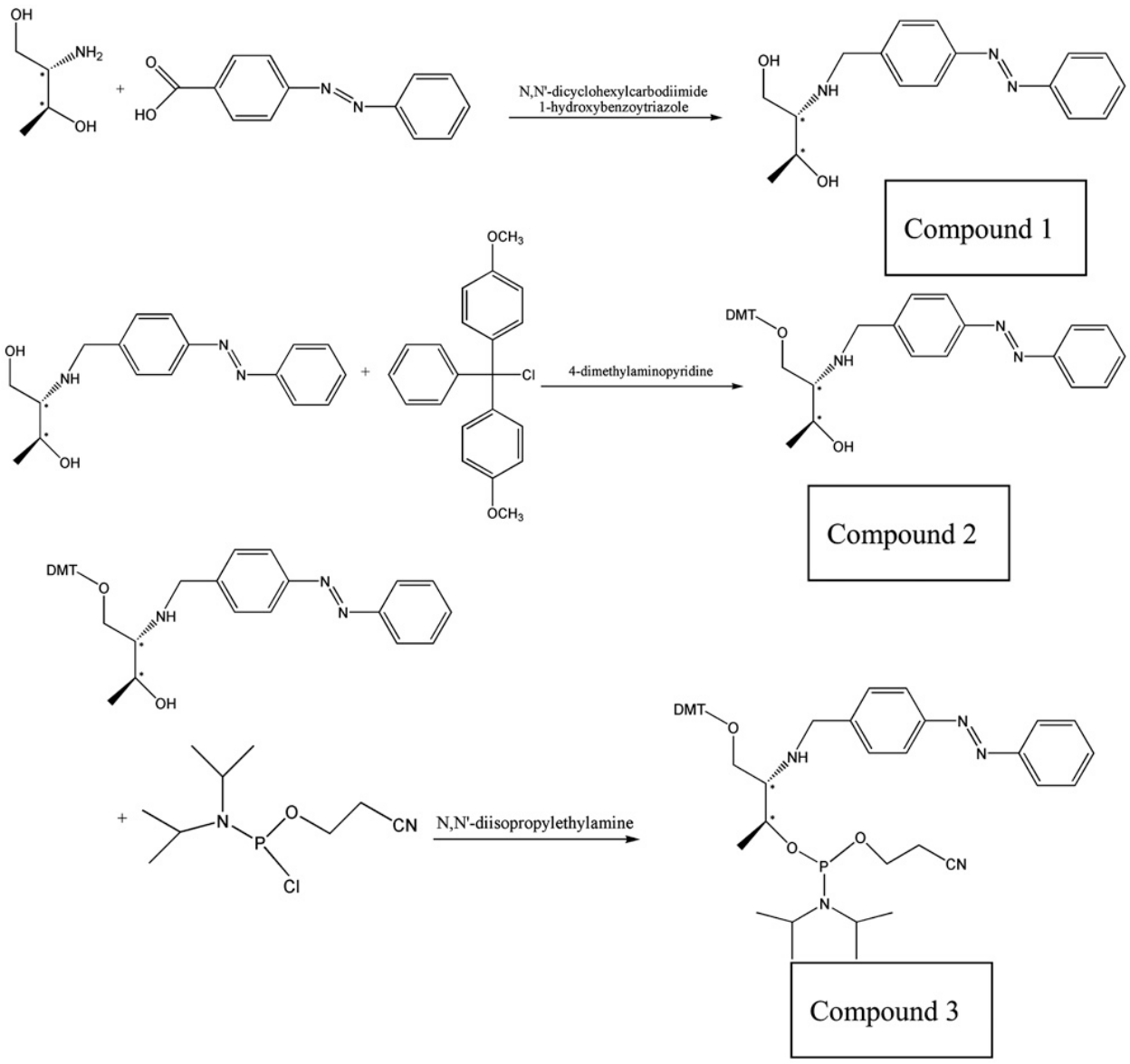

Figure 2-3. Synthesis procedure of azobenzene phosphoramidite[46].

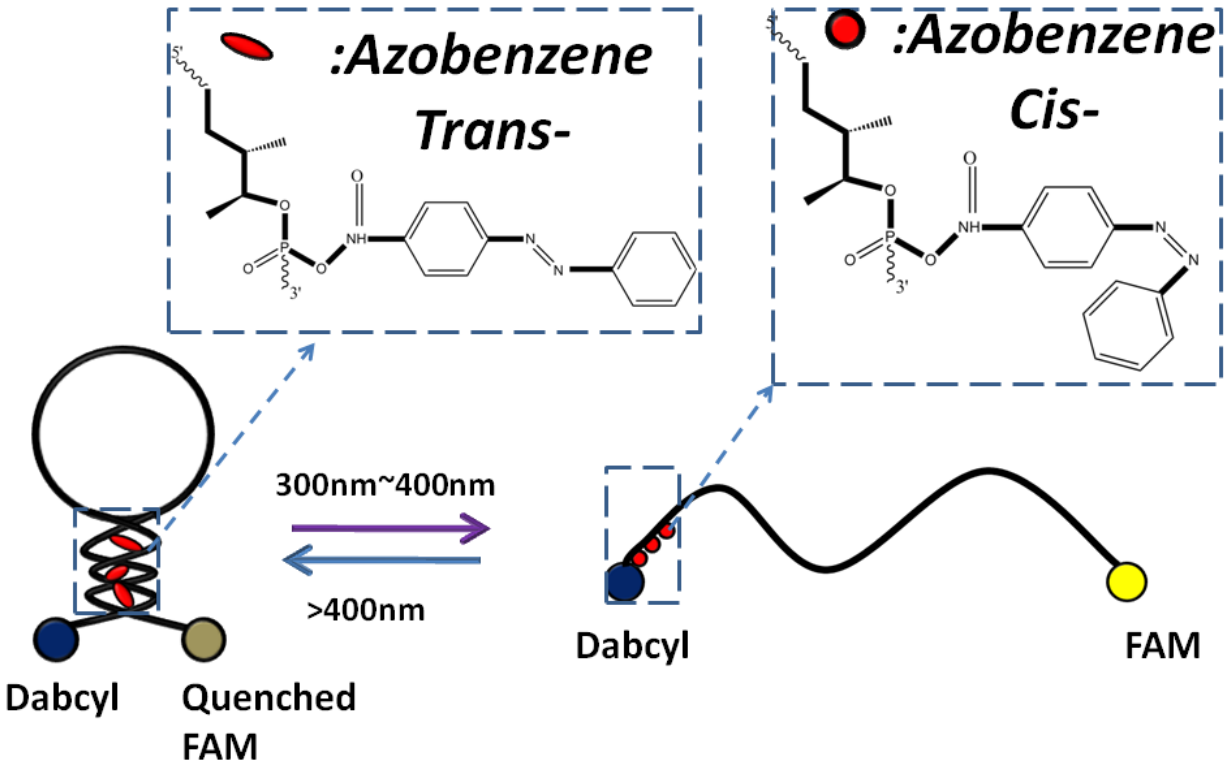

Figure 2-4. Open-close conversion of DNA nanomotor with three azobenzene moieties. 3' side of DNA labeled with Dabcyl as quencher while 5' side labeled with FAM.

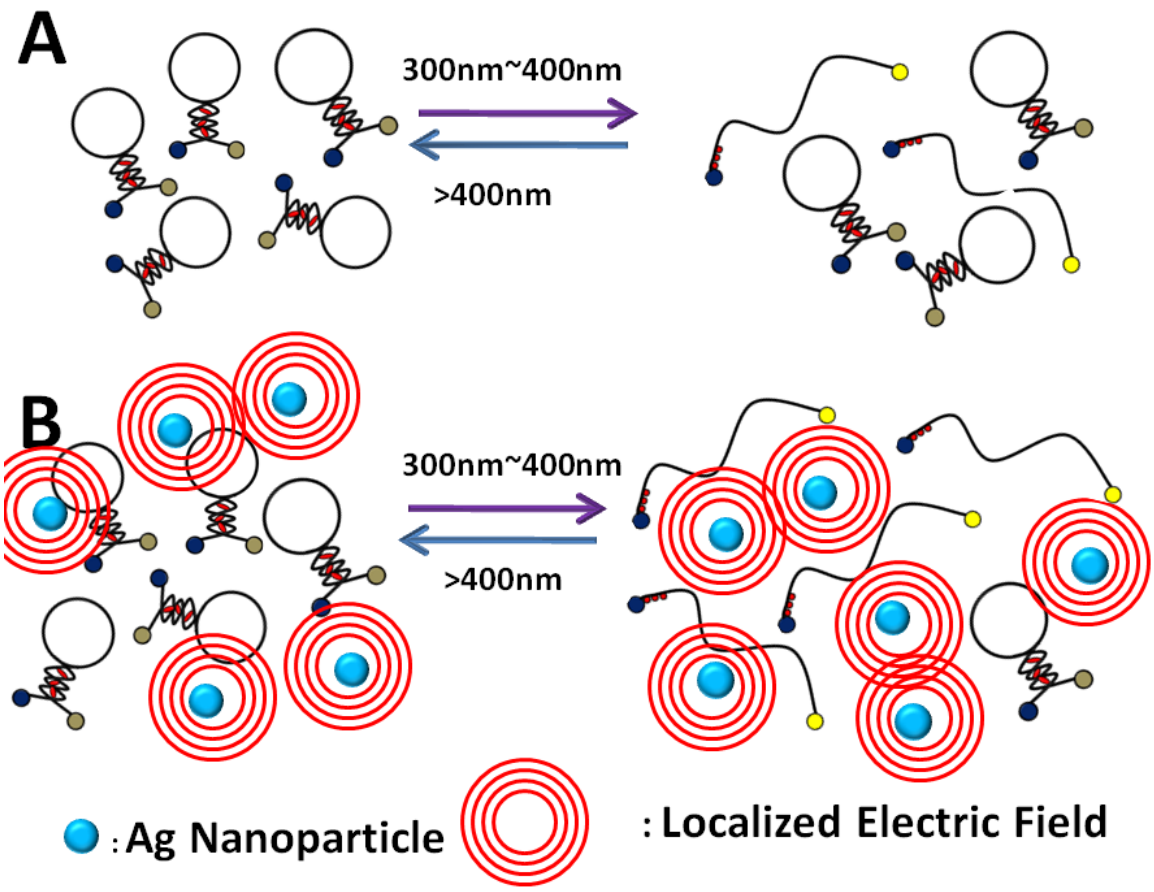

Figure 2-5. Scheme of the enhanced DNA nanomotor. A) DNA nanomotor shown low conversion efficiency without Ag nanoparticle. B) DNA nanomotor's conversion efficiency was enhanced by Ag nanoparticle's localized electric field.

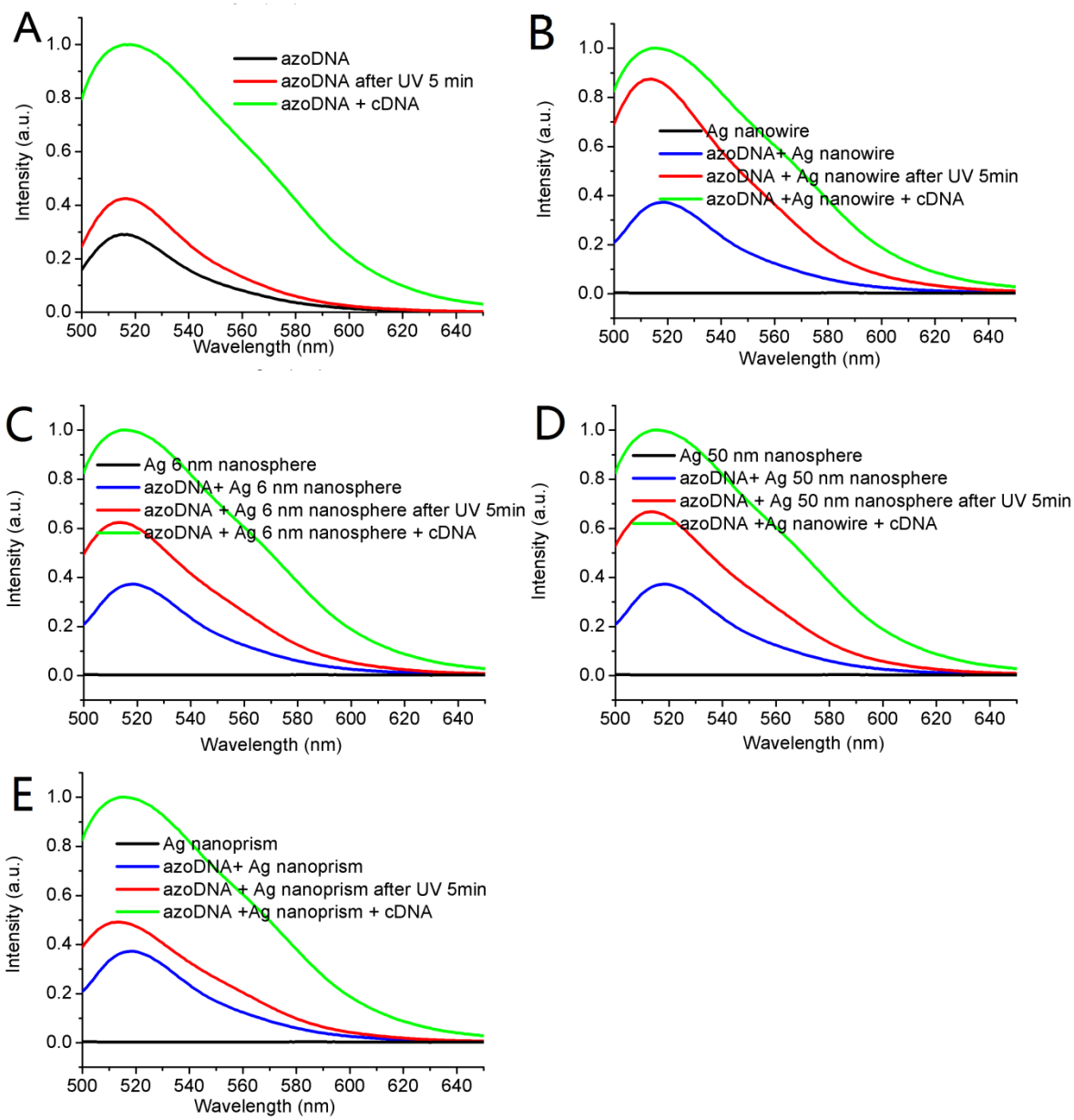

Figure 2-6. Fluorescence spectra of DNA nanomotor (λ_{ex} = 488 nm) incubated with A) DNA only. B) Ag nanowires (40 μm). C) Ag nanospheres (6 nm). D) Ag nanospheres (50 nm). E) Ag nanoprisms (side length of 50 nm).[46].

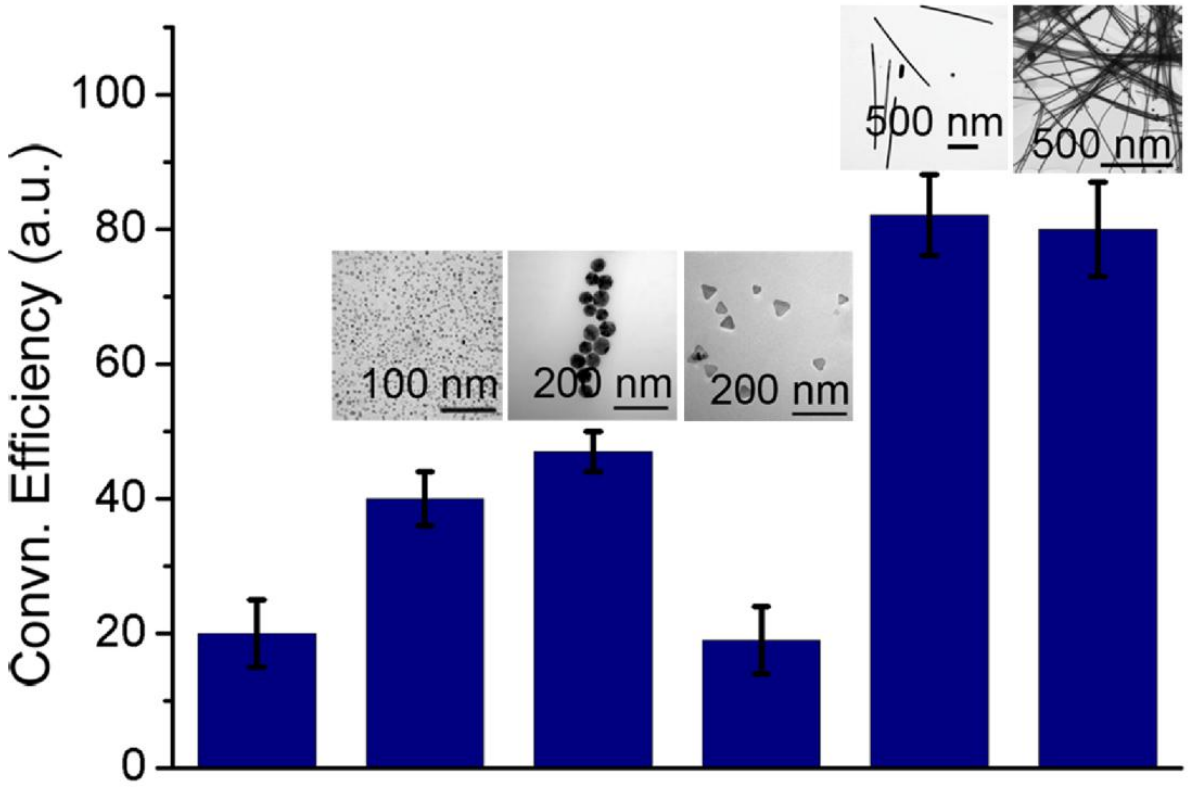

Figure 2-7. Conversion efficiency of DNA nanomotors in the existence of Ag nanomaterials with different morphologies[46].

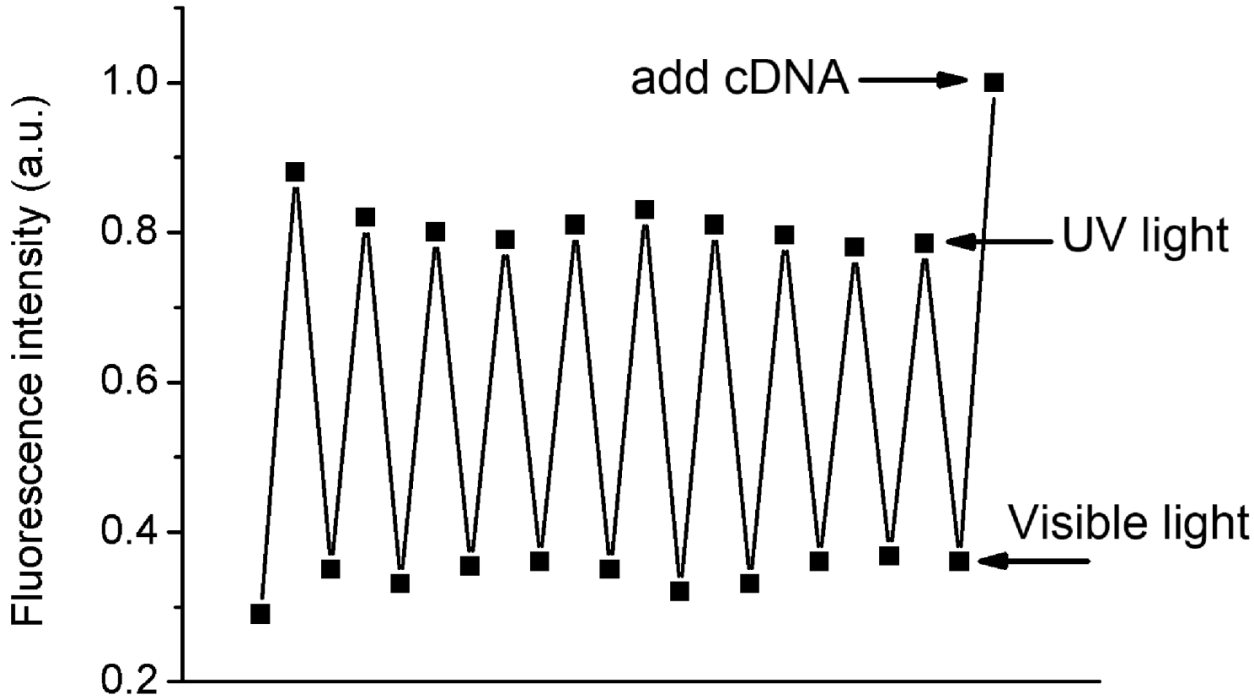

Figure 2-8. Reversible conversion of DNA nanomotor with Ag nanowire. Each cycle: UV (350 nm), 5 min; Vis (450 nm),5 min.[46]

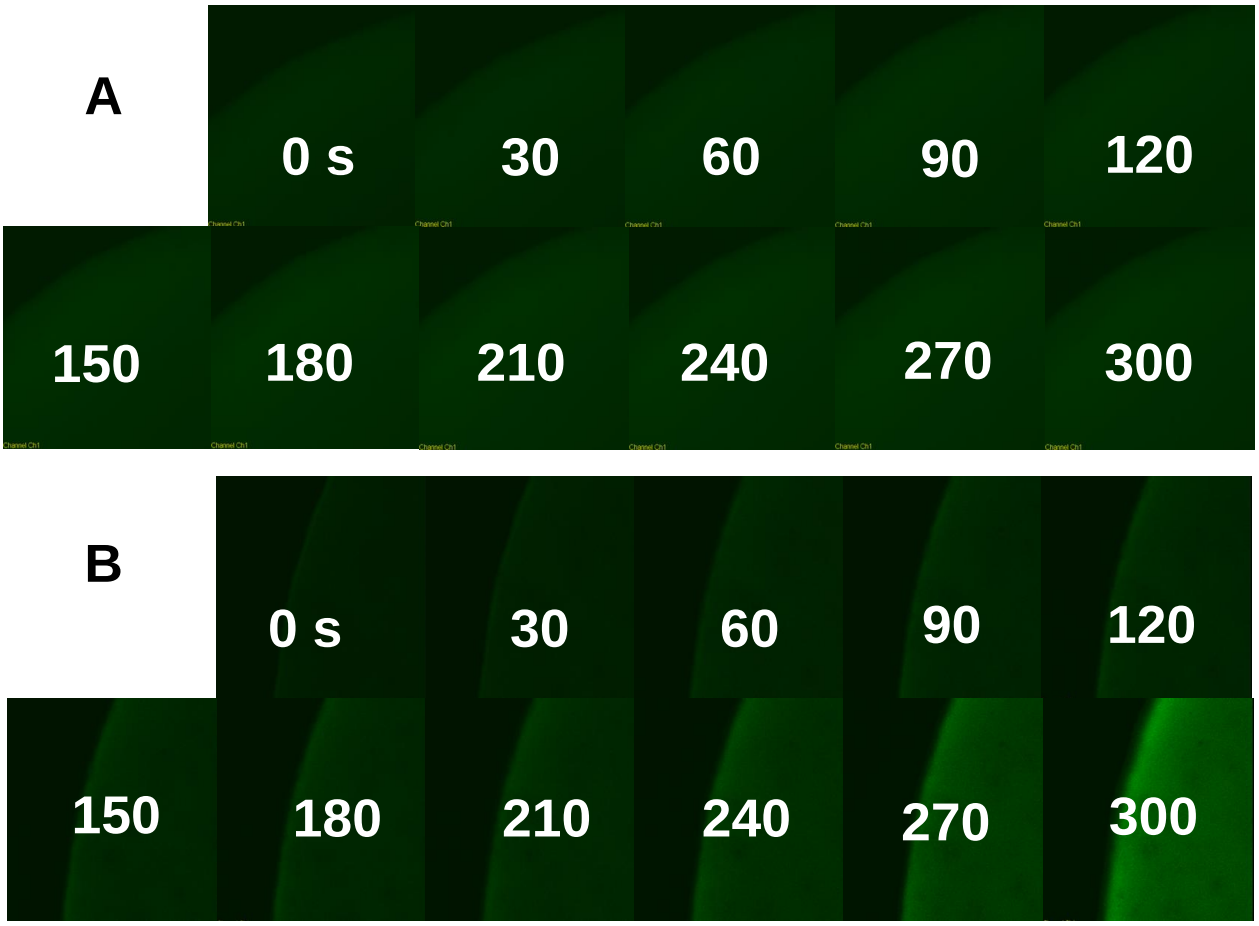

Figure 2-9. Fluorescence micrographs of DNA nanomotor solution. A) DNA nanomotor only. B) DNA nanomotor with Ag nanowire under UV irradiation. Image taken from confocal microscopy.[46]

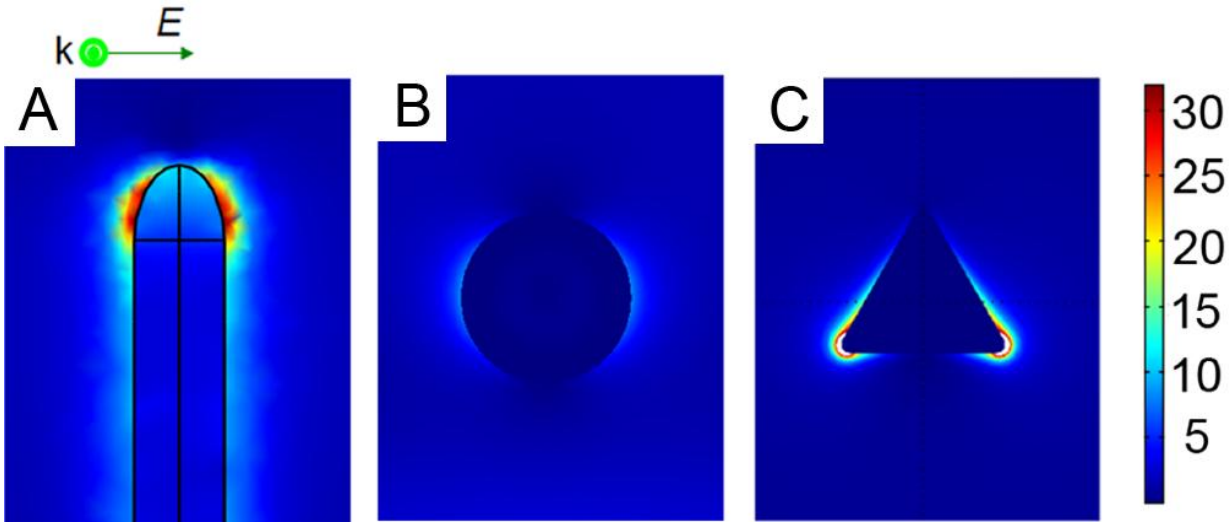

Figure 2-10. Localized electric field intensity distributions ($|E|^2$) calculated for A) Ag nanowire (1 μm). B) Ag nanosphere (50 nm). C) Ag nanoprism (50 nm)(calculated at irradiation wavelength of 350 nm)[46].

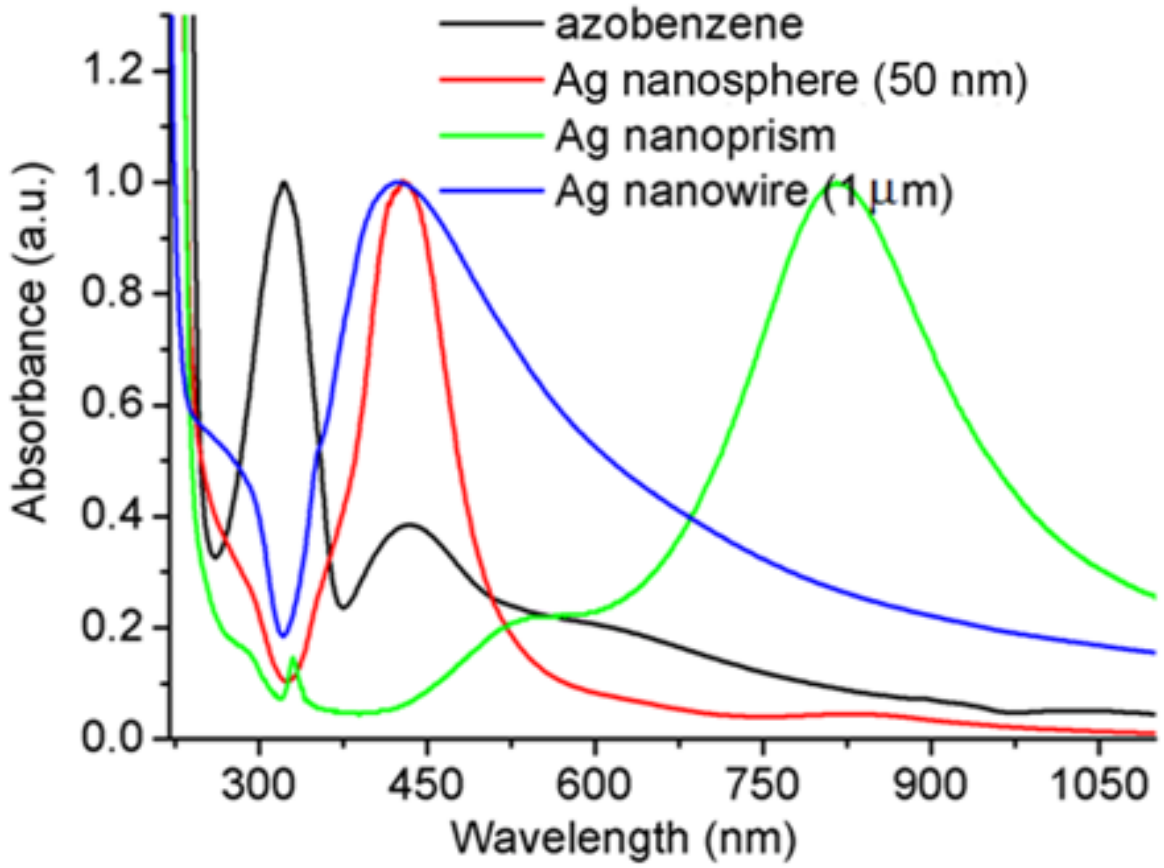

Figure 2-11. Extinction spectrum of Ag nanostructures and absorption spectrum of azobenzene molecule[46].

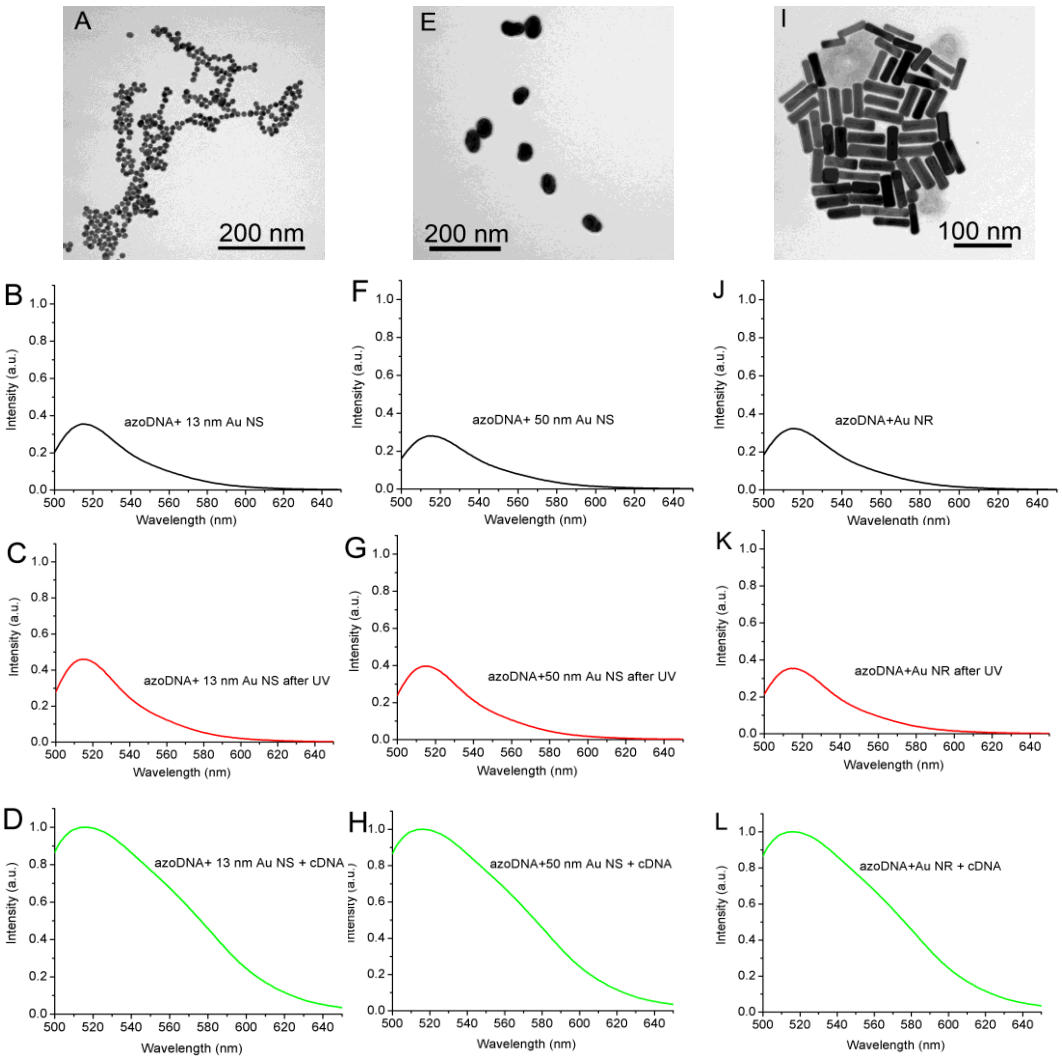

Figure 2-12. Image of Au nanoparticle and fluorescence spectrum of DNA motor. A) Image of Au nanosphere (13 nm). B) Fluorescence spectrum of DNA motor incubated with Au nanosphere (13 nm). C) Fluorescence spectrum of DNA motor incubated with Au nanosphere (13 nm) after 5 min UV irradiation. D) Fluorescence spectrum of DNA motor incubated with Au nanosphere (13 nm)with excess cDNA. E) Image of Au nanosphere (50 nm). F) Fluorescence spectrum of DNA motor incubated with Au nanosphere (50 nm). G) Fluorescence spectrum of DNA motor incubated with Au nanosphere (50 nm) after 5 min UV irradiation. H) Fluorescence spectrum of DNA motor incubated with Au nanosphere (50 nm)with excess cDNA. I)Image of Au nanorod (60 nm x13 nm). J) Fluorescence spectrum of DNA motor incubated with Au nanorod (60 nmx13 nm). K) Fluorescence spectrum of DNA motor incubated with Au nanorods (60 nmx13 nm) after 5 min UV irradiation. L) Fluorescence spectrum of DNA motor incubated with Au nanorods (60 nmx13 nm)with excess cDNA[46].

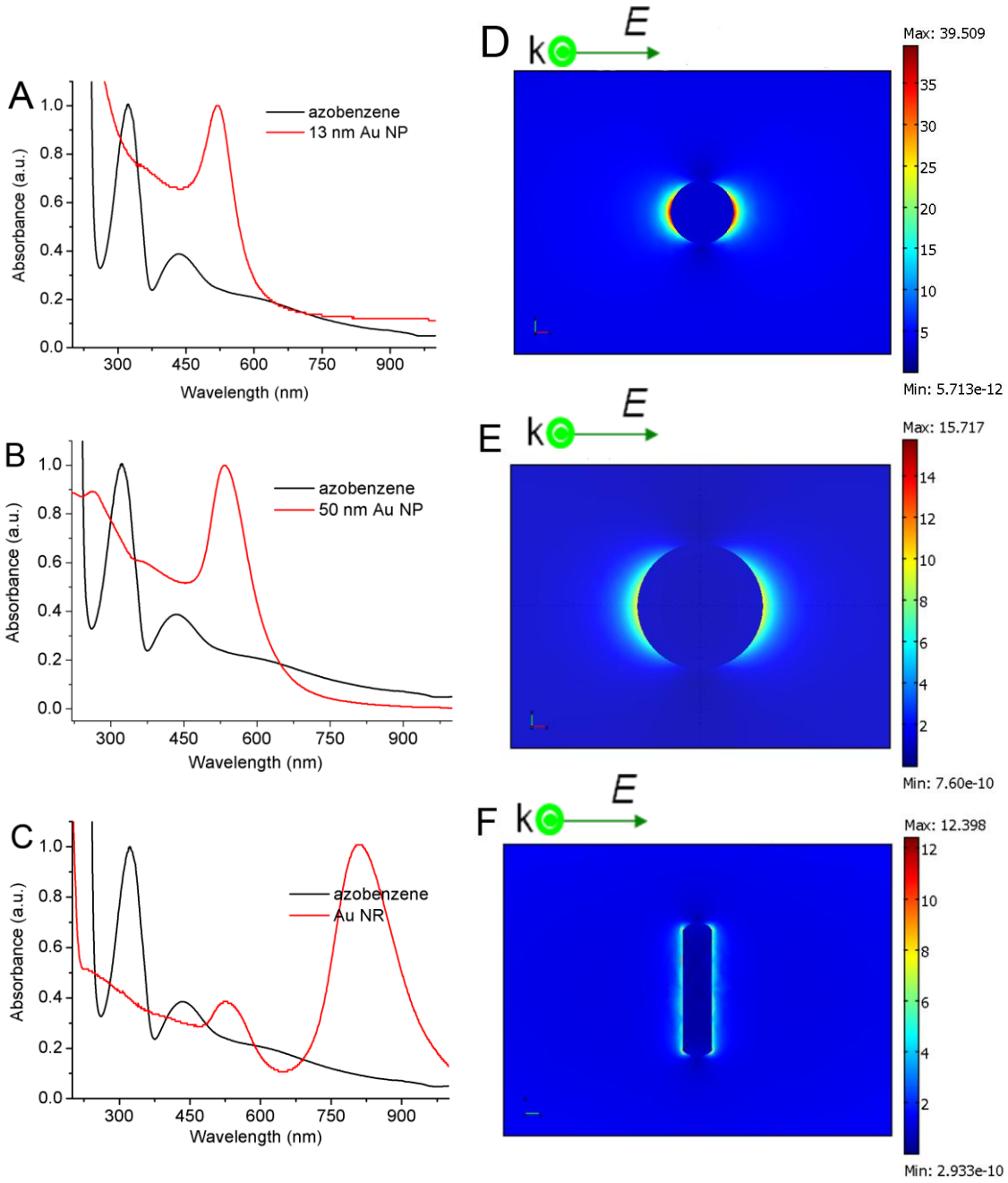

Figure2-13. The experimental extinction spectrum of Au nanoparticle with absorption spectral of azobenzene. A) Au nanosphere (13 nm). B) Au nanosphere (50 nm). C) Au nanorod(13 nm × 60 nm). Theoretical calculated electric field distributions ($|E|^2$) was calculated at wavelength of 350 nm. D) Au nanosphere (13 nm). E) Au nanosphere (50 nm). F) Au nanorod (13 nm × 60 nm)[46].

Table2-1. Sequence of azobenzene nanomotor, normal nanomotor, and complimentary DNA to nanomotor.

Sequence Name	Sequence(Azo for Azobenzene Phosphoramidite)
Azobenzene DNA Nanomotor	5’-FAM-CCT-AGC-TCT-AAA-TCA-CTA-TGG-TCG-C-Azo-GC-Azo-TA-Azo-GG-Dabcyl-3’
Normal DNA	5’-FAM-CCT-AGC-TCT-AAA-TCA-CTA-TGG-TCG-CGC-TAG-G-Dabcyl-3’
cDNA	5’-GGA-TCG-AGA-TTT-AGT-GAT-ACC-AGC-GCG-ATC-C-3’

CHAPTER 3
USING LIGHT DRIVEN DNA STRANDS FOR THE PHOTO CONTROLLED REVERSIBLE RELEASE SYSTEM OF MESOPOROUS NANOCONTAINER

Stimuli-responsive nucleic acids with specific geometry change respond to external stimuli, such as pH[8], metal ion[47,48], light source[12] have already shown their great potential in molecular sensing, logic gate operation[49], and nanomachine design[12]. In previous research we have developed a high conversion efficiency light driven DNA nanomotor. In this project, we combine the technique of light-driven DNA motor and Mesoporous silica nanoparticle to investigate a new light control reversible release system.

Based on stable structure, lack of cytotoxicity, bio-compatible, large inner space, ease of surface-modification and homogeneous pore size distribution, mesoporous silica have recently been rapidly developed as a controlled release system for guest molecules[24-29,34,35]. In most cases guest molecules will be released with the external stimuli to mesoporous silica nanoparticle and this process is not reversible. Compared to target molecule stimuli, photo control release has significant advantages of fast response and ease of control without loss of efficiency. In addition, by switching the irradiance source a reversible controlled-release process can be realized. In this chapter, we report a new photo controlled responsive DNA/mesoporous silica hybrid release system by introducing light sensitive azobenzene DNA nanomotor to the surface of mesoporous material.

Experimental Section

Chemicals

The chemicals tetraethylorthosilicate(TEOS), n-cetyltrimethylammonium bromide (CTABr), 3-(Triethoxysilyl)propyl isocyanate(TSPI),sodium hydroxide(NaOH), Sodium

Nitrate(NaNO3), 3-(N-morpholino)propanesulfonic acid (MOPS), Triton X-100, Rhodamine 6G, anhydrous toluene, ethanol, methanol were provided by Sigma-Aldrich. Fluorescein was provided by Invitrogen. De-ionized water was obtained from Milli-Q pump. Phosphate buffered saline (PBS) and tris(hydroxymethyl)aminomethane (Tris) were purchased from Fisher Scientific.

Instrumentations

Fluorescence measurements were carried out on a FluoroLog-3 spectrofluorometer (Jobin Yvon). The concentrations of all DNAs were calculated by measuring the absorbance of DNA at 260 nm on a Cary Bio-300UV spectrometer (Varian), as the extinction coefficient was calculated on Integrated DNA Technologies website. The extinction coefficient of the azobenzene moiety was calculated as 4,100 M^{-1}/cm^{-1} [12]

Scanning electron microscopy (SEM) images were taken from a JEOL JSM-6700 scanning electron microscope. Transmission electron microscopy (TEM) images were obtained on an H-7000 NAR transmission electron microscope (Hitachi) with a working voltage of 100 kV.

XRD patterns were recorded on a D/MAX-2000 diffractometer (Rigaku), using Cu-Kα radiation (λ= 1.5406 Å).The nitrogen adsorption and desorption isotherms at 78.3 K were measured using an ASAP 2010 analyzer (Micromeritics). The BET model was applied to evaluate the specific surface areas. Pore size and pore volume were determined from the adsorption data by the BJH method.

Synthesis of Azobenzene Phosphoramidite

Azobenzene phosphoramidite was synthesized according to the protocol reported by Asanuma et al[10]. The detailed synthesis procedure was described in chapter 2.

Synthesis and Purification of DNA Sequences

The azobenzene-modified DNA sequences were synthesized using an ABI3400 DNA/RNA synthesizer (Applied Biosystems). The synthesis started with a controlled pore glass (CPG) column at 1 μmole scale. The azobenzene phosphoramidite coupling reagent was prepared by dissolving in acetonitrile at 20 mg/200 μL for single incorporation. A 15-min coupling time was used to improve the synthesis yield. DNA products were cleaved from CPG by incubating with 2mL 1:1 Ammonium hydroxide/ Methylamine (AMA) for 30min in a 65^{o}C water bath. Then the cleaved DNA was precipitated by adding 250μL 3.0M NaCl and 6.25mL ethanol and kept in -20^{o}C freezer overnight. Then the precipitated DNA was dissolved in 400μL trithylamine acetate (TEAA) for the next purification step.

The DNA was purified in a C18 column on Varian Prostar HPLC machine. The collected DNA solution was dried in a vacuum dryer and then detritylated in 80% acetic acid for 30mins. Then 500μL ethanol with 20μL 3M NaCl was added to detritylated DNA again. The ethanol supernatant was removed and then the DNA was dissolves in 400μL de-ionized water. The concentration of DNA was calculated by measuring the absorbance of DNA solution, while the extinction coefficient of each sequence was calculated on Integrated DNA Technologies website. The molar extinction coefficient of the azobenzene moiety was calculated as 4,100 M^{-1}/cm^{-1} [12]. All the DNA products were kept in -20^{o}C freezer. Note that all the azobenzene products should avoid all kinds of direct light irradiation. All the DNA sequences used in this project are listed in Table 3-1.

Synthesis of Mesoporous Silica Nanoparticle

CTAB (1.00 g, 2.74 mmol) was dissolved in 480 mL of nanopure water with 3.50 mL 2.00 M sodium hydroxide aqueous solution in a 1L flask. The solution was stirred by a magnetic stir bar and the temperature of the mixture was adjusted to 80 ^{o}C. 5.00 mL of the TEOS solution (22.4 mmol) was added drop by drop to the surfactant solution under vigorous stirring. The reaction was kept at 80 ^{o} C for 2 h to give a white precipitate. This solid product was filtered, washed with deionized water and methanol for more than 3 times, and dried in air to yield the as-synthesized mesoporous silica nanoparticles (denoted as MSN). To remove the surfactant template (CTAB), 1.50 g of the as-synthesized MSN was refluxed for 24 h in a methanolic solution of 9.00 mL of HCl (37.4%) in 160.00 mL methanol. The resulting material was filtered and extensively washed with deionized water and methanol again.

Surface Functionalize of Mesoporous Silica Nanoparticle with Short DNA

1.00g MSN was refluxed in 80.00 mL of anhydrous toluene with 0.25 mL of 3-isocyanatopropyltriethoxysilane for 20 h to get surface functionalized with 3-isocyanatopropyl group (noted as MSN-NCO). After discarded the toluene by centrifuge, the purified MSN-NCO (100 mg) was dispersed in 2 mL of de-ionized water, certain amount of 200 μM amine-modified Arm-DNA (5'-T-A-C-C-T-A-NH2-3') were then added. Then the mixture was shake in a incubate overnight at room temperature to allow the amino groups of DNA react with the -NCO functional groups on the surface of MSN(noted as MSN-DNA).

Dye Loading and DNA Capping of Mesoporous Silica Nanoparticle

50 mg MSN-DNA was added to 5 mL 5.00 mM Rhodamine 6G solution in 1X PBS buffer (pH = 7.4). After the mixture was shaking overnight in a dark room, the final

mixture was then centrifuged and washed with PBS buffer solution three times. The azobenzene-modified-ssDNA (noted as azo-DNA 1 mL, 120 μM) was added to hybridize with arm-DNA on MSN and cap the pores on the mesoporous particles(noted as MSN-R6G). Then the capped MSN was washed again to remove the dye absorbed on the surface.

The maximum amount of Rhodamine 6G loaded on the MSN was determined by analyzing the supernatant solution spectrophotometrically. All the washing solutions were collected, and the loading amount was calculated. Compared to the initial concentration of rhodamine 6G solution, the maximum loading amount of rhodamine 6G was approximately 47 μmol per gram MSN.

Irradiation Sources

A 6 W UV light source was chosen as the UV light source to convert the azobenzene from *cis*- to *trans*- transition (DNA dehybridize, MSN uncap). As the visible light source, a 60 W table lamp with a 450 nm filter was selected to cause the azobenzene converse from *cis*- to *trans*- (DNA hybridize, MSN cap). For all the experiments, the light sources were carefully positioned to avoid the heating effect on the samples.

Characterization of the DNA modified Mesoporous Silica Nanoparticle (MSN-DNA)

The size and morphology of Mesoporous silica nanoparticle nanoparticle were characterized by Transmission Electron Microscopy (TEM) and Scanning Electron Microscopy (SEM). The TEM image was taken on a Hitachi H-7000 NAR transmission electron microscope under a working voltage of 100 kV. The high definition image were shown from Figure 3-1. Scanning electron microscopy (SEM) images were taken from a JEOL JSM-6700 scanning electron microscope (Figure 3-2).

The porosity of the Mesoporous silica nanoparticle was characterized by XRD. XRD patterns were recorded on a D/MAX-2000 diffractometer (Rigaku), using Cu-Kα radiation (λ= 1.5406 Å).The XRD pattern was shown in Figure3-3.The nitrogen adsorption and desorption isotherms at 78.3 K were measured using an ASAP 2010 analyzer (Micromeritics) (Figure3-4). The BET model was applied to evaluate the specific surface areas. Pore size and pore volume were determined from the adsorption data by the BJH method.(Pore size distribution see Figure 3-5, Surface area and pore volume calculation results see Table 3-2)

Dye Release Experiment of DNA Capped MSN-R6G

Dye loaded DNA-modified-MSN (MSN-R6G) was dispersed in Tris buffer (20 mM Tris-HCl, 20 mM NaCl, 2 mM $MgCl_2$, pH = 8). In each release experiment, 0.5mg MSN-R6G was kept in a mini dialysis tube (cut off molecular weight= 7,000),and tube was immersed in a 10ml beaker with 5ml same buffer(shown in Figure3-6). During the dye release process, the released dye could disperse through the dialysis membrane, while the MSN and DNA would be kept inside tube. Samples were taken from the solution in beaker, and the dye release process was monitored by measuring the fluorescence intensity.

Results and Discussion

Light driven molecule azobenzene and its derivatives isomerizes from the *trans*- to *cis*- forms under irradiation at 300–380 nm and isomerizes from *cis*- to *trans*- under irradiation at wavelengths > 400 nm[42]. For the double strand azobenzene DNA, the azobenzene phosphoramidite in *cis*- form(under UV irradiation)would cause the dehybridization of the duplex and it will reverse back with the irradiation of visible light[12].

It has been already reported that by the geometry change of the DNA attached on the pore of mesoporous silica nanoparticle, the open-close of the pore can be controlled[8].

In this project azobenzene DNA was used to cap the mesoporous silica nanoparticle, as shown in Figure 3-7, single-stranded Arm-DNA (5'-T-A-C-C-T-A-3') was attached on the pore edge of mesoporous silica particle. The linker DNA azo-DNA strands with azobenzene moieties (azo-DNA) was hybridized to the arms. Under visible light irradiation (λ = 450 nm), the azobenzene moieties were in the *trans*- form, and the linkers kept hybridized to the arms, then the pores were tightly capped, and the loaded guest molecule was trapped in mesoporous particle . Switched the irradiation source to UV light (λ = 365 nm), the azobenzene moieties converted to the *cis*- form. This would cause the dehybridization between Arms and azo-DNA and the pores were uncapped. Because of the reversibility of azobenzene molecule, the process was also reversible as if the irradiation source switched back to visible light, the azo-DNA would hybridize with Arm DNA again to cap the pore.

Dye Release Test under Different Irradiation Source

The dye release process under different irradiance was monitored by measuring the fluorescence intensities measured on fluorescence spectroscopy as a function of time. The experimental procedure has been described before. As shown in Figure 3-8, under the irradiation of visible light (450 nm), the fluorescence intensity increased very slowly that no obvious dye release was observed, indicating that the mesoporous particle was well capped by azo-DNA and dye was trapped well without leaking. When the irradiation source was switched to UV (365 nm), the fluorescence intensity of the released dye in solution increased rapidly and reached 91% release after 1500 min. This result showed that the azo-DNA capped mesoporous silica nanoparticle was a

good carrier for guest molecule, and rapidly response to the UV irradiation which lead to a large release of guest molecule.

For comparison, a normal DNA without azobenzene modification was also used to cap mesoporous silica particle and dye release test was taken under UV and visible irradiation. However, no dye release was detected after UV irradiation (Figure 3-9).

Optimization of azo-DNA Sequences

To optimize the design of azo-DNA sequence with a better response to UV irradiation, DNA strands (azo-DNA-1/azo-DNA-2/azo-DNA-3/azo-DNA-4), sequences shown in Table3-1) were prepared with different numbers and positions of azobenzene moieties. Dye release from mesoporous silica nanoparticle capped with each sequences was tested. As shown in Figure 3-10, azo-DNA-4 gave the best release results, so this sequence was used in the entire project.

Reversibility of Dye Release System

One significant advantage of this release system was the reversibility of open-close cycles of pores via alternating irradiation wavelengths. As shown in Figure 3-11, started with visible irradiation only a very small amount of released dye was detected, while a rapid increase of released dye was detected when the irradiation wavelength was suddenly changed from visible(450nm) to UV light (365 nm) at 120 min. At 240 mins when changing the irradiation source back to visible light at 450 nm, the pore was capped again and release of the trapped dye was sonly restricted, and this cycles could be repeated for many times. The release process shows that the on-off switching is reversible and can be repeated several times with a good reversibility.

Conclusion

In this project we have developed a photo controlled reversible release system by capping mesoporous container with light-sensitive DNA strand. The photo-sensitive “capping/uncapping” release system sensitively response to different irradiations, then exhibited a light controlled release process. After the optimization of azo-DNA strands 91% of cargo release can be reached after 1500 mins release time. This “capping/uncapping” was reversible by switching different irradiation sources with a rapid response and high reversibility after several cycles.

This new design already showed a great potential toward the development of light controlled guest molecule release systems. Therefore, rapid switching between the open and closed states can be used to control drug release, which can be great help in a wide range of desired applications, especially for targeted drug delivery to avoid the side effects.

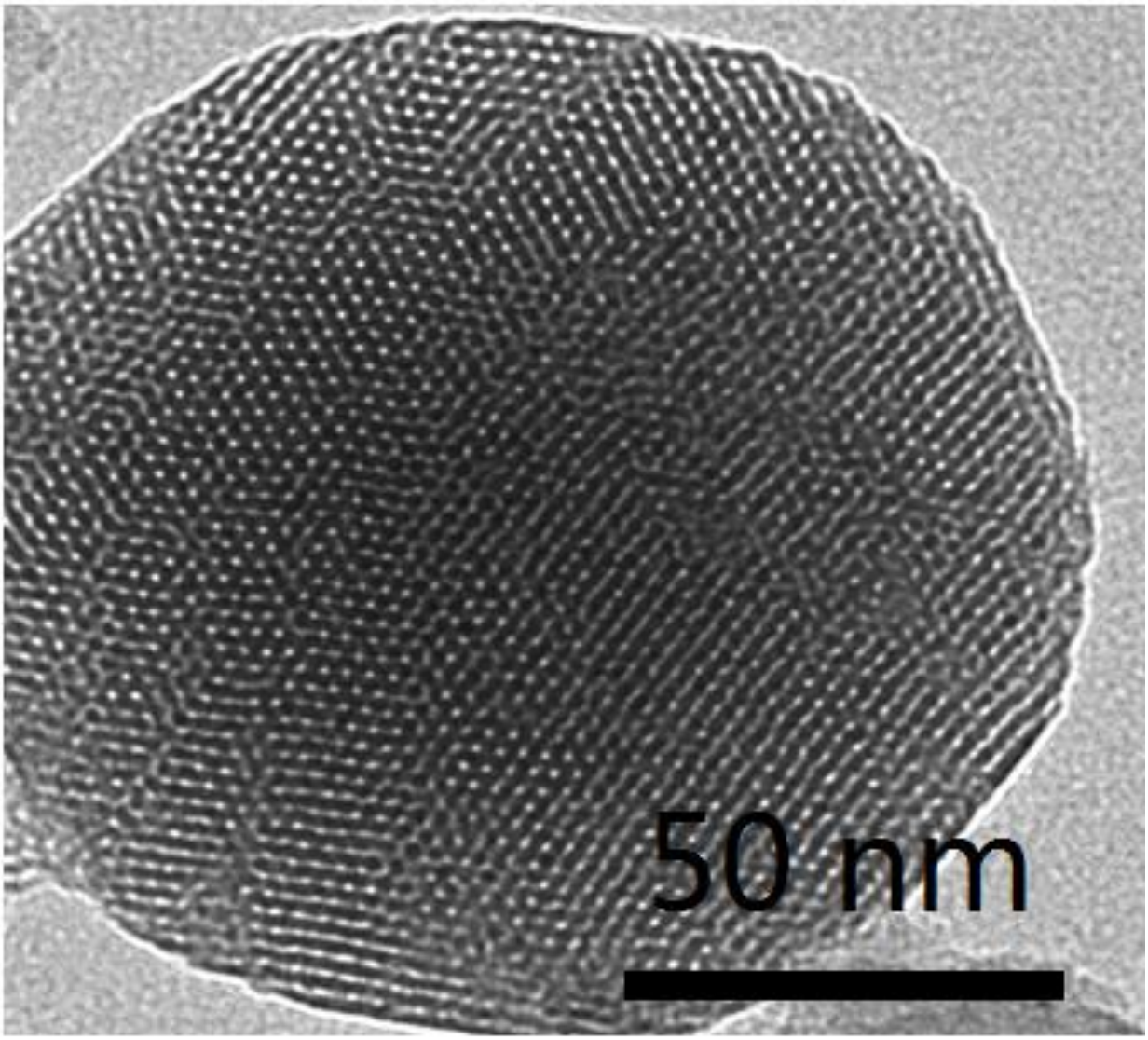

Figure 3-1. TEM image of DNA-modified-MSN.

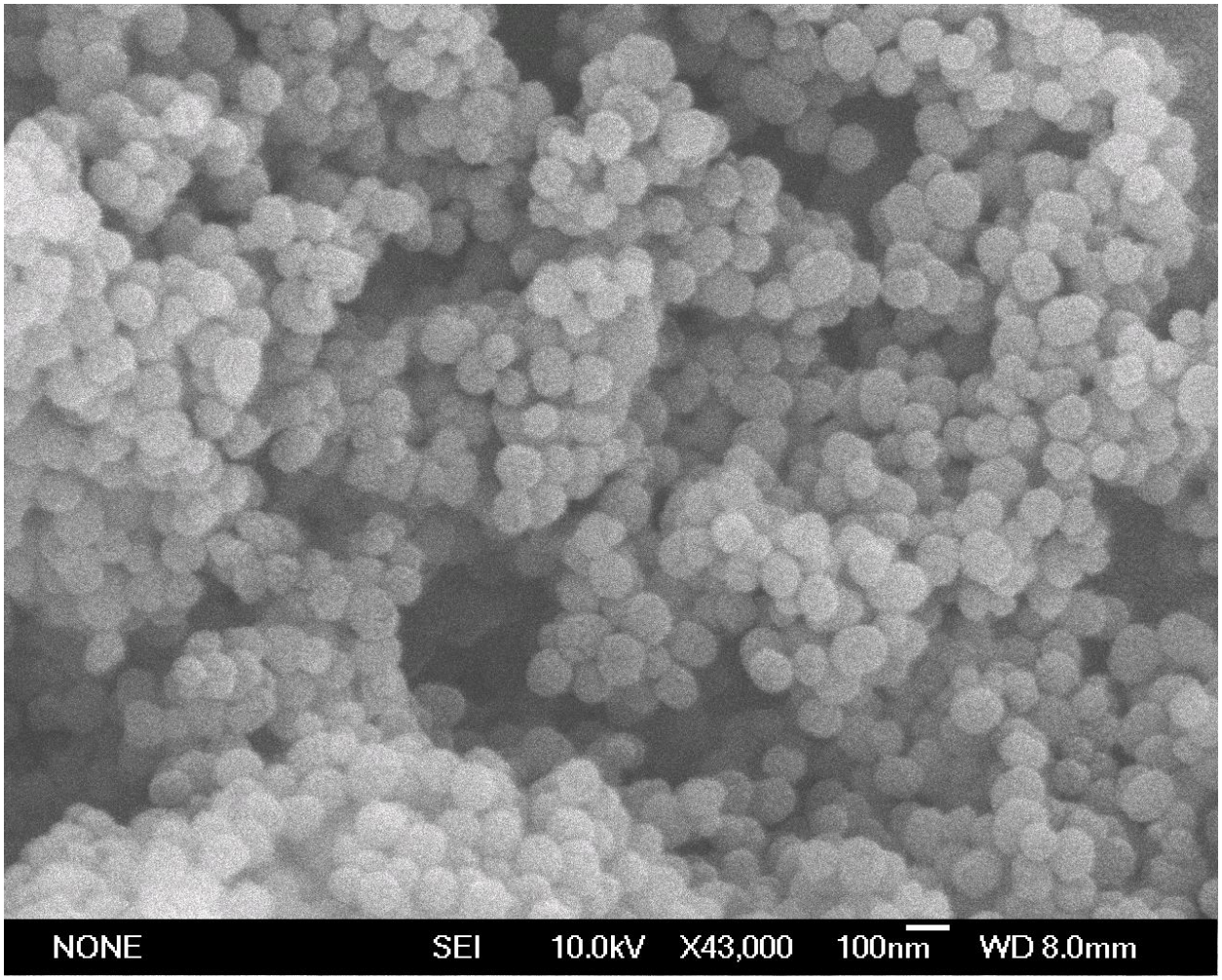

Figure 3-2. TEM image of DNA-modified-MSN.

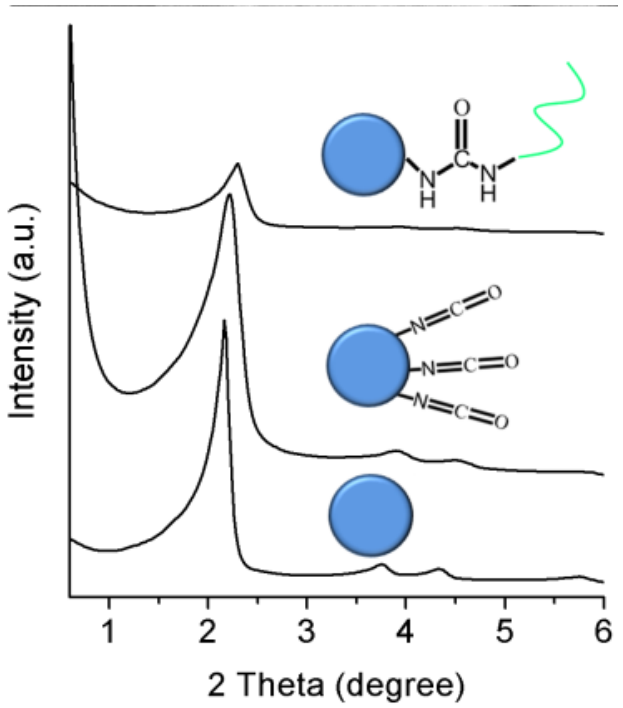

Figure 3-3. Small-angle XRD pattern of MSN, MSN-NCO, and MSN-DNA.

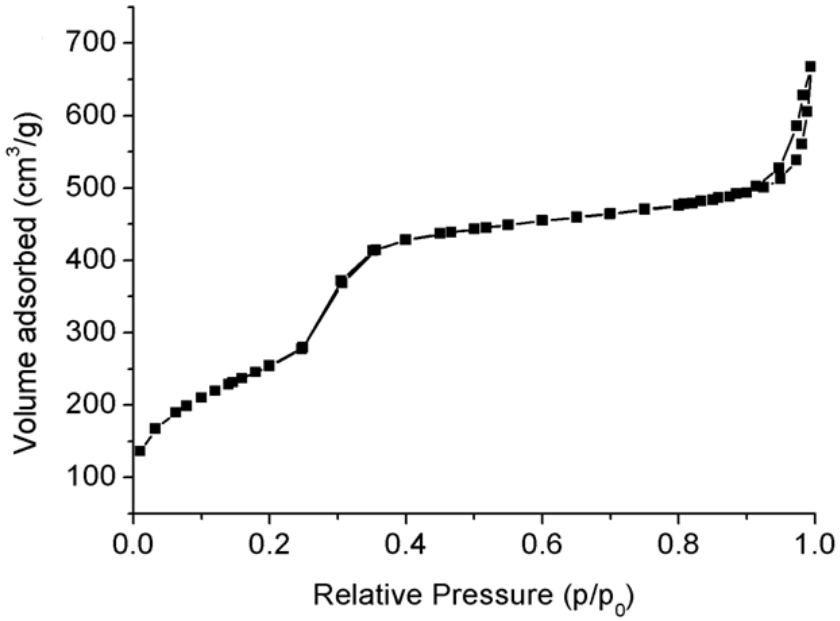

Figure 3-4. BET nitrogen adsorption/desorption isotherms of DNA functionalized mesoporous silica nanoparticle(MSN-DNA).

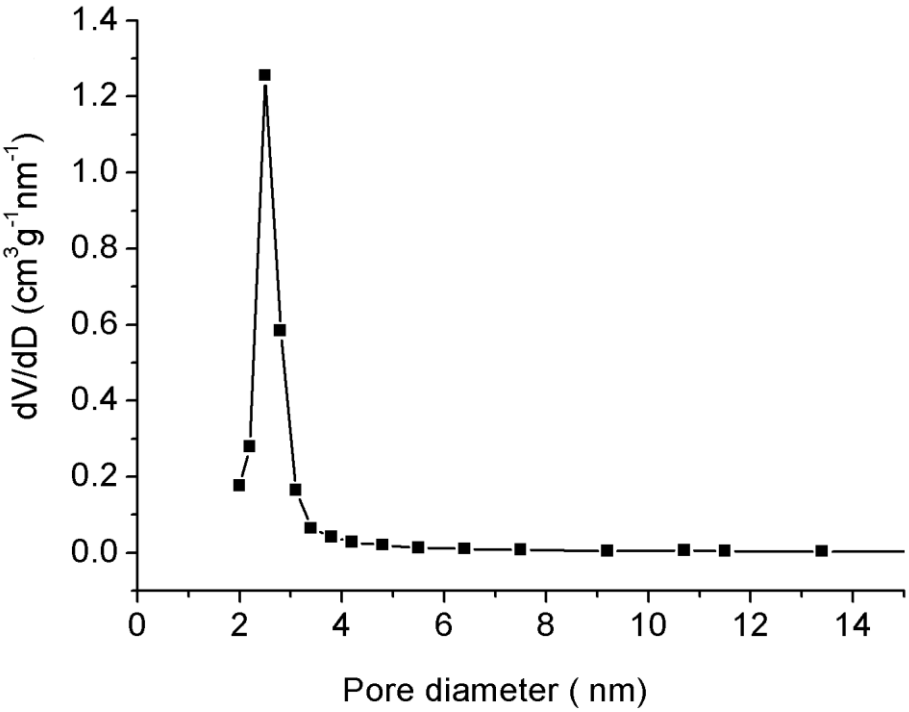

Figure 3-5. BJH pore size distributions of DNA-functionalized mesoporous silica nanoparticle (MSN-DNA).

Figure 3-6. The setup of the mesoporous dye release device.

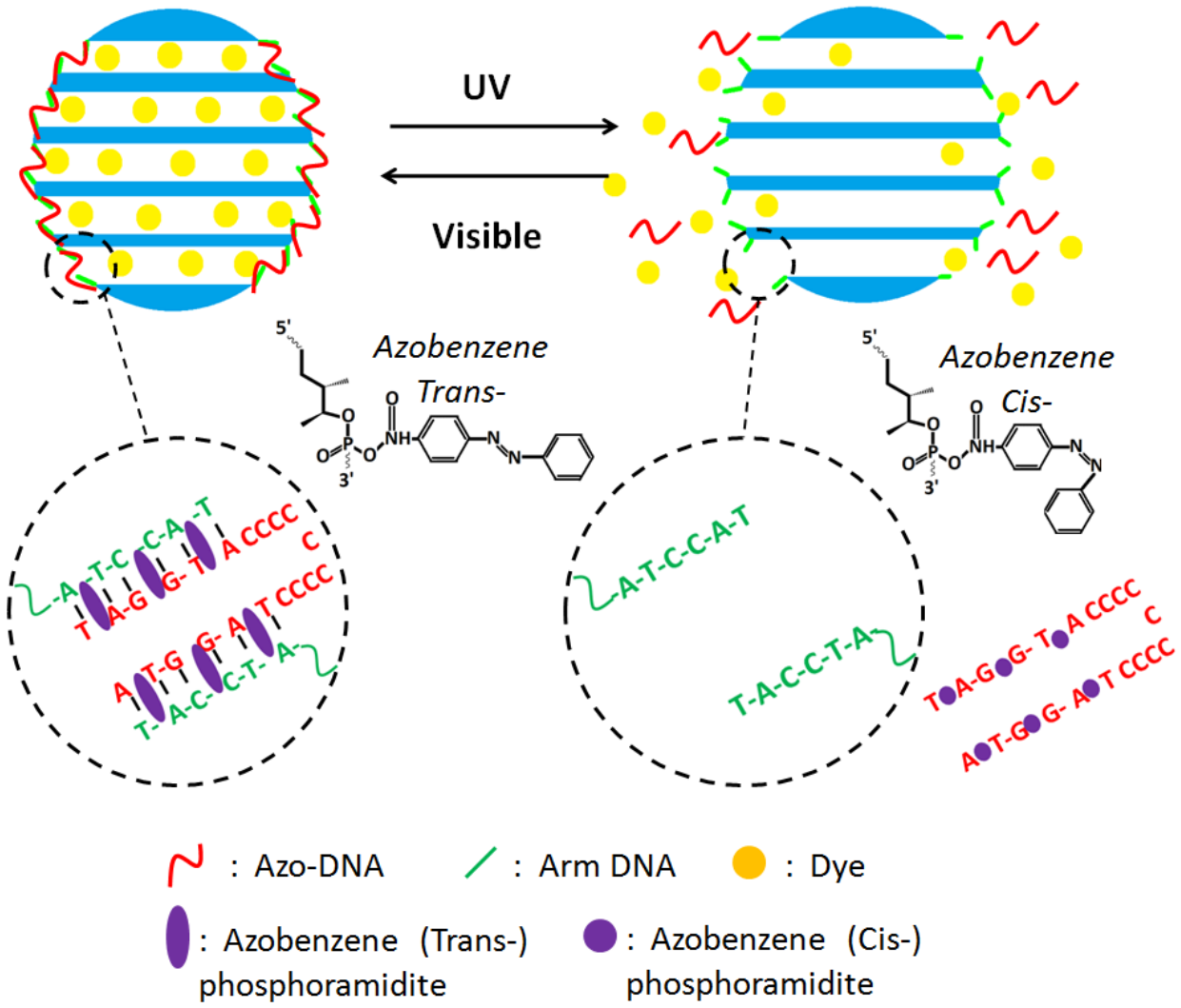

Figure 3-7. The scheme of azobezene-modified DNA based light driven reversible release system.

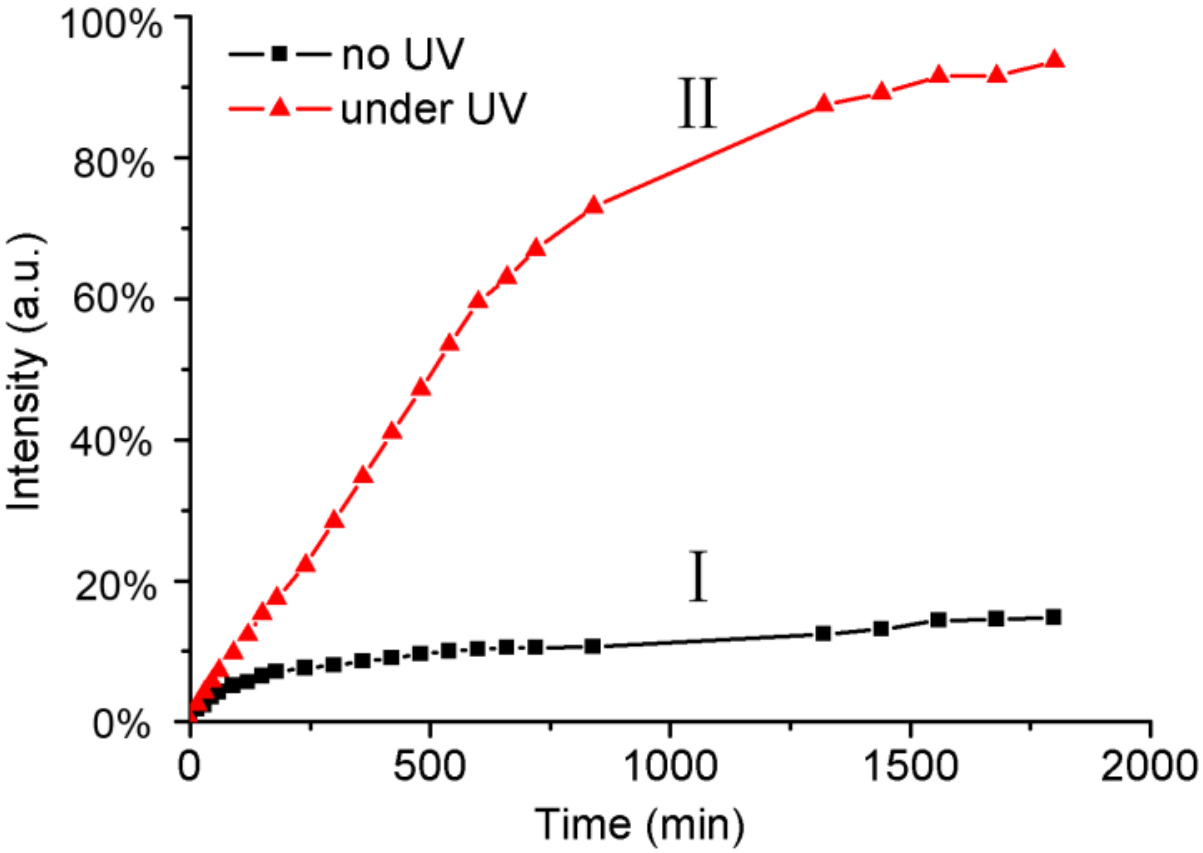

Figure 3-8. Time dependent rhodamine 6G release curves from DNA capped mesoporous silica nanoparticle under different irradiation. Fluorescence intensities have been normalized to the maximum level of dye released.

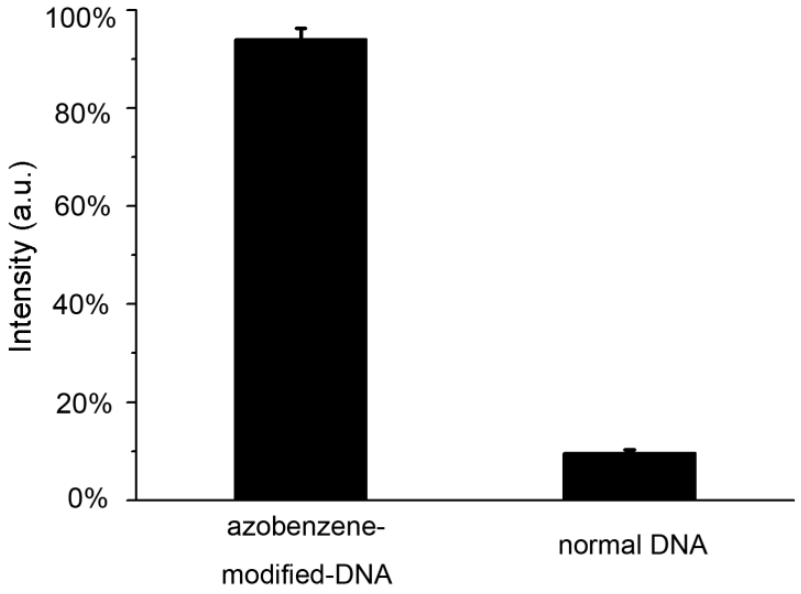

Figure 3-9. Dye release under UV irradiation from mesoporous particle with azo-DNA and normal DNA for 1500 min, data were normalized to the maximum of dye released in the experiment.

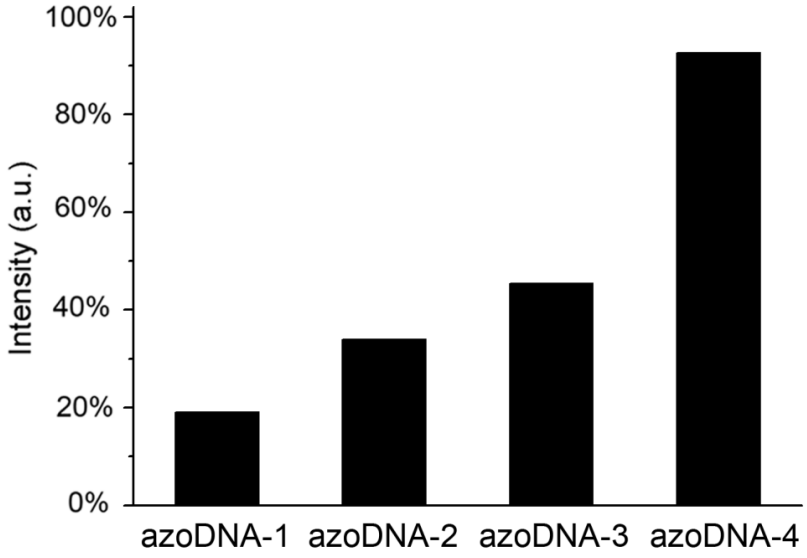

Figure 3-10. Dye release under UV irradiation from mesoporous particle with azo-DNA1/ azo-DNA2/ azo-DNA3/ azo-DNA4 for 1500 min, data was normalized to the maximum of dye released in the experiment.

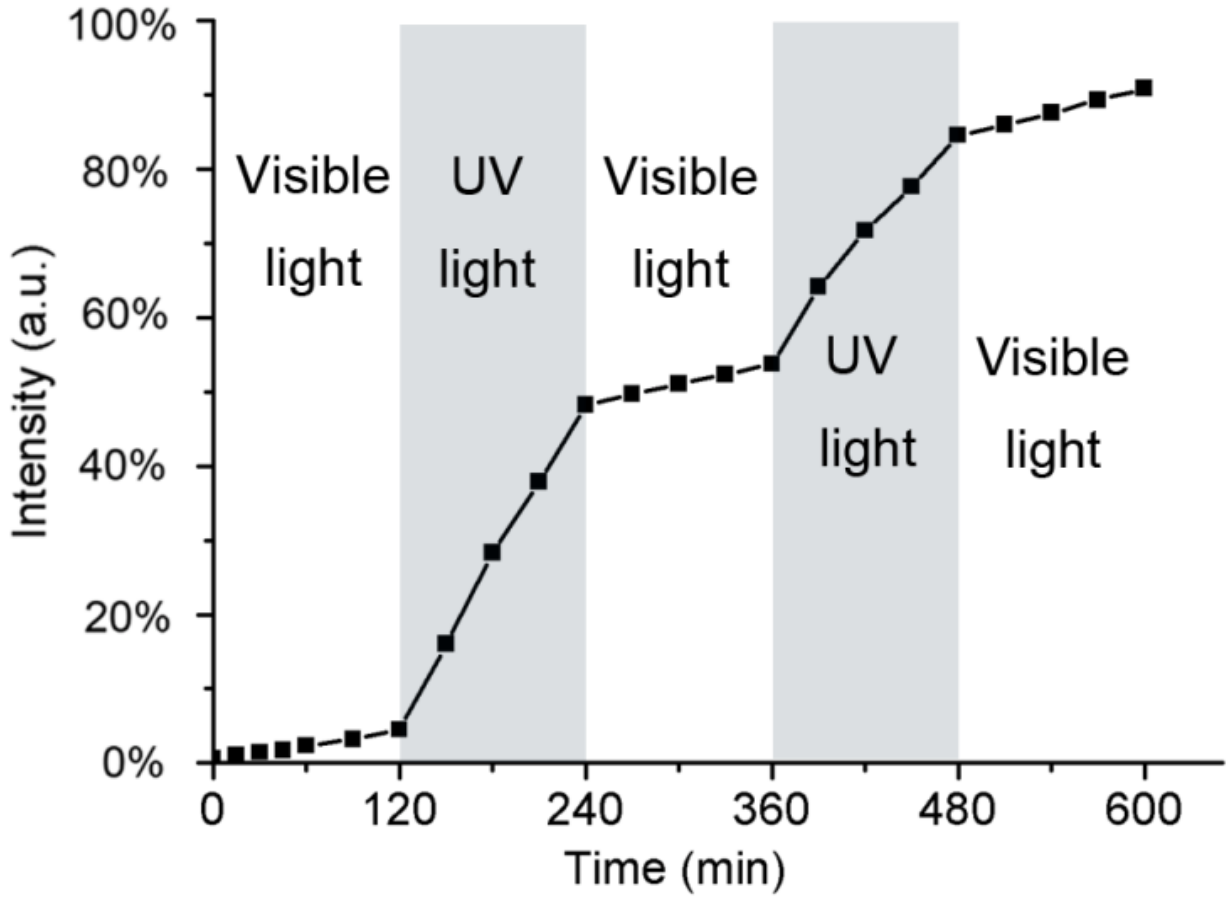

Figure 3-11. Dye release curve from MSN as a function of time while switching irradiation source every 120 mins, showing the reversible capping/uncapping control of mesoporous particle by changing the irradiation wavelength. Data was normalized to the maximum of dye released.

Table3-1. Sequence of Azobenzene DNA, normal DNA, and arm DNA.

Sequence Name	Sequence(Azo for Azobenzene Phosphoramidite)
azo-DNA-1	5'-T-A-G-G-**Azo**-T-A-CCC-CCC-CCC-CCC-T-A-G-G-**Azo**-T-A-3'
azo-DNA-2	5'-T-A-**Azo**-G-G-**Azo**-T-A-CCC-CCC-CCC-CCC-T-A-**Azo**-G-G-**Azo**-T-A-3'
azo-DNA-3	5'-A-**Azo**-T-A-**Azo**-G-G-**Azo**-T-A-CCC-CCC-CCC-CCC-A-**Azo**-T-A-**Azo**-G-G-**Azo**-T-A-3'
azo-DNA-4	5'-T-**Azo**-A-G-**Azo**-G-T-**Azo**-A-CCC-CCC-CCC-CCC-T-**Azo**-A-G-**Azo**-G-T-**Azo**-A-3'
Normal DNA	5'-T-A-G-G-T-A-CCC-CCC-CCC-CCC-T-A-G-G-T-A-3'
Arm-DNA	5'-T-A-C-C-T-A-NH_2-3'

Table 3-2. Surface area and pore volume of Mesoporous silica nanoparticle before surface modification (MSN), after surface modification and DNA conjugation(MSN-DNA), and after dye loading(MSN-R6G).

Sample	Surface area(m^2/g)	Pore volume(m^3/g)
MSN	842.27	1.0322
DNA-functionalized-MSN (MSN-DNA)	628.38	0.79572
Rh6G-loaded-MSN (MSN-R6G)	502.45	0.82572

CHAPTER 4
USING ION SENSITIVE DNA STRANDS FOR THE DETECTION OF MERCURIC ION ON A MESOPOROUS STIMULI-RELEASE SYSTEM

Mercury pollution is a global contamination problem with varies of nature origins and seriously harmful to human's health [50]. This problem is attracting more and more attention and concern from society due to mercury's high toxicity at low concentration, and the bioaccumulative property in human's body. Even little amount of mercury could cause severe damage to kidney, nervous system and other organs[51]. The mercury can be accumulated in human body through several processes, and one of the major source is the water soluble Hg^{2+} ion contamination in drinking water. In 2001 The United States Environmental Protection Agency (EPA) has acclaimed the top limit of 2 ppb (10 nM) for Hg(II) in drinking water[52]. Therefore, developing a new mercuric ion detection methods which is sensitive, easy to operate, low-cost and applicable to aqueous system becomes important and urgent[53].

There are many traditional methods for the detection of mercuric ion in aqueous systems, but almost all of them require complicated sample preparation and expensive instruments such as atomic absorption spectroscopy, cold vapor atomic fluorescence spectrometry, and gas chromatography[53]. In order to simplify the sample preparation and reduce the cost on the instrument , many mercuric ion detection methods have been developed basing on small organic molecules like fluorophores[54], nanoparticle like gold nanosphere[14,55] or biomaterials such as DNAzymes[48], DNA hydrogel[15] and protein[56]. The original mechanism of these approaches basicly rely on directly binding or reaction between the probe and Hg^{2+} that causes the detectable color or fluorescence change[57].

In this project we designed a DNA functionalized mesoporous silica nanoparticle based Hg^{2+} responsible dye release system to realize the direct, fast, sensitive detection of Hg^{2+} in aqueous system. The detection was realized by capping the mesoporous silica nanoparticle (MSN) with Hg^{2+} sensitive DNA to trap the dye inside and releasing dye molecule inside MSN in the existence of $Hg^{2+.}$ We made use of the unique structure of MSN as the carrier of the dye and use T-base rich DNA as the mercuric ion responsible cap for MSN. In our design we capped MSN by a Hg^{2+} sensitive DNA T-rich strands to trap the dye molecule inside MSN, and when immersed in solution with Hg^{2+}, pores on MSN would be opened and dye would be released. By measuring the fluorescence intensity of released dye a detection of Hg^{2+} was realized.

Experimental Section

Chemicals

The chemicals tetraethylorthosilicate(TEOS), n-cetyltrimethylammonium bromide(CTABr), 3-(Triethoxysilyl)propyl isocyanate(TSPI),sodium hydroxide(NaOH), Sodium Nitrate($NaNO_3$), 3-(N-morpholino)propanesulfonic acid (MOPS), Triton X-100, Rhodamine 6G, Mercury(II) Acetate($HgAc_2$), Lead(II) Acetate($PbAc_2$), Barium(II) Acetate($BaAc_2$), Iron(II) Acetate ($FeAc_2$), Iron(III) Chloride ($FeCl_3$), Zinc(II) Acetate($ZnAc_2$), Magnesium Acetate($MgAc_2$), Cadmium(II) Acetate($CdAc_2$), Copper(II) Acetate($CuAc_2$), Cobalt(II) Acetate ($CoAc_2$), Nickel(II) Acetate($NiAc_2$), Calcium(II) Acetate($CaAc_2$), anhydrous toluene, ethanol, methanol were provided by Sigma-Aldrich. Fluorescein was provided by Invitrogen. De-ionized water was obtained from Milli-Q.

Buffer Solutions

Binding buffer consisting in 10 mM MOPS, 50 mM $NaNO_3$ 0.05%(in volume)Triton X-100 (pH=7.0) was used for DNA binding and dye release experiences

Hybridization buffer in 10 mM MOPS, 50 mM $NaNO_3$ 20mM $MgAc_2$(pH=7.0) was used for DNA hybridization.

Synthesis of Mesoporous Silica Nanoparticle

The MCM-41 mesoporous silica nanoparticle was prepared by the following procedure: 500mg n-cetyltrimethylammonium bromide(CTABr) was dissolved and suspended in 250ml DI water. Then 3.5ml NaOH (1M) was added. The CTABr solution was transferred to a 500ml triple neck bottle, then heated to 80 degree with the magnetic stirring. After while 2.5ml tetraethylorthosilicate(TEOS) was added drop by drop to the CTABr solution. Then reaction was taken for 2 hour with magnetic stirring to obtain the write powder precipitate. The mixture was cooled down under room temperature, then centrifuged at 2000rpm for 10 min to get rid of the supernant . The solid was washed with ethanol for three times. The final product was reflux in methanol for 20 hours to get rid of CTABr. After washed with ethanol three times the product mesoporous silica nanoparticle (MSN) was obtained and kept dried under room condition.

Surface Modification and Dye Loading of Mesoporous Silica Nanoparticle

1g extracted MSN was refluxed in 80ml anhydrous toluene with 0.25ml 3-(Triethoxysilyl) propyl isocyanate(TSPI) for 20hours to immobilize the isocyanate group on the surface. The isocyanate-functionalized MSN(MSN-NCO) was collected and washed with anhydrous toluene three times, then dried in oven under 70^{o} to evaporate toluene. The 1g functionalized MSN-NCO was suspended in 20ml 2.5mg/ml Rhodamine 6G water solution inside a 50ml centrifuge tube to load the dye in the pores of MSN-NCO scaffolding. The mixture was ultrasonic for 1min then shake 24hours with aim to achieving maximum dye loading. Afterward the dye-loaded MSN-NCO was washed

quickly with ethanol for three times and dried in oven under 70^{o} C. The dye-loaded MSN-NCO(MSN-R6G) was kept dried until next step.

Characterization of Mesoporous Silica Nanoparticle

The size and morphology of Mesoporous silica nanoparticle nanoparticle were characterized by Transmission Electron Microscopy (TEM) and Scanning Electron Microscopy (SEM). The TEM image was taken on a Hitachi H-7000 NAR transmission electron microscope under a working voltage of 100 kV. The high definition image were shown from Figure 4-1. Scanning electron microscopy (SEM) images were taken from a JEOL JSM-6700 scanning electron microscope (Figure 4-2).

The porosity of the mesoporous silica nanoparticle (MSN), surface functionalize mesoporous silica nanoparticle(MSN-NCO) and dye loaded mesoporous silica nanoparticle(MSN-R6G) were characterized by XRD. XRD patterns were recorded on a D/MAX-2000 diffractometer (Rigaku), using Cu-Kα radiation (λ= 1.5406 Å).The XRD pattern was shown in Figure4-3.

Synthesis and Purification of DNA Sequences

All the DNA sequences used in this project are listed in Table 4-1. Three DNA sequences were all synthesized on ABI 3400 DNA synthesizer. The synthesis process was similar to the process in chapter 3 and 4. Debcyl CPG was used for the synthesis of Linker-DNA and Amino CPG was used for the synthesis of Arm-DNA. All the DNA products were deprotected and cleaved from CPG by incubating with 2mL 1:1 Ammonium hydroxide/ Methylamine for 20 min in a 65^{o}C water bath. After while the supernatant was transferred to a 15mL eppendorf tube. 250μL 3.0M NaCl and 6.25mL ethanol were added to help the precipitation of DNA. The mixture were kept in -20^{o}C

until most of the DNA precipitated to bottom. After while the mixture was centrifuged to get rid of the supernatant solution, and the precipitated DNA was redissolved in 400μL trithylamine acetate (TEAA) for the next step.

The DNA was purified on Varian Prostar HPLC machine through a C18 column. The purified DNA should also be detritylated in 80% acetic acid for at least 30mins. Then the detritylated DNA was precipitated in 500μL ethanol with 20μL 3M NaCl. The mixture was kept in -20^{o}C freezer until most of the DNA precipitate again. The ethanol supernatant was removed and then the DNA was dissolved in 400μL de-ionized water. The concentration of DNA was calculated by measuring the absorbance of DNA solution, while the extinction coefficient of each sequence was calculated on Integrated DNA Technologies website. All the DNA products were kept in -20^{o}C freezer, the Fluorefore-Linker-DNA with the FAM coupling should be kept in dark and avoid all kind of irradiations.

Adjustment of Short DNA on Particle Surface

In order to confirm the maximum amount of Arm-DNA to saturate the surface of dye loaded mesoporous silica nanoparticle, the saturation titration of Arm-DNA has benn tested on MSN-R6G. Certain amount (2uL/4uL/8uL/12uL/16uL/20uL/24uL) of 1mM Amino-modified Arm-DNA solution was added to 1mg MSN-R6G in a 1.5ml centrifuge tube. Binding buffer was added to adjust the overall volume to 200uL. The mixture was kept shaking overnight in incubator under room temperature (with speed 1000rpm). Afterward the mixture was centrifuged and the supernatant was separated from particle.

The amount of Arm-DNA attached on the MSN was calculated by the absorbance change of the supernatant. From the titration curve(see Figure 4-4), 12nmol of Arm-DNA was the optimal amount to saturate the surface of 1mg MSN-R6G, while around 10nmol of Arm-DNA would finally bind on the surface of MSN-R6G.

For the preparation of solid MSN-Arm-DNA, 500μg MSN-R6G was suspended in 200μL binding buffer containing 6nmol of the amino modified Arm-DNA. The suspension was ultrasonic for 30min then shake in an incubator overnight (1000rpm, room temperature). The solution was centrifuged and washed with binding buffer for three times. This step was operated fast to avoid the free release of the Rhodamine 6G from the particle. The absorbance of the supernatant was measured to calculate the binding efficiency of Arm-DNA which was in the range of 85.71%-90.63%.

DNA Capping of the Mesoporous Silica Nanoparticle

After the binding of the Arm-DNA on the surface of the dye loaded Mesoporous silica nanoparticle, the Linker-DNA was introduced to hybridize with the Arm-DNA immobilized on the MSN then cap the pore. 500μg MSN-Arm-DNA solid was suspended in 200μL hybridization buffer with 20nmol of Linker-DNA. The solution was shake in an incubator for 2 hours(1000rpm, room temperature), then centrifuged and the supernatant was kept. The particle was washed with binding buffer for three times. The absorbance of the supernatant was measured to calculate the hybridization efficiency of Linker-DNA to the Arm-DNA. According to the calculation results 22.37%-23.29% of the Linker DNA was hybridized to the Arm-DNA, which means the ratio of Linker-DNA to Arm-DNA on the MSN is from 2.23:1.00 to 2.14:1.00. From the result one

Linker-DNA will bridge link two Arm-DNA on the surface of the MSN, which was exactly the expect result.

Quenching effect of Mercuric Ion on Different Organic Dyes

In order to confirm the dye used in mercuric ion detection system would not be quenched by the mercuric ion itself, the quenching effect of different organic dyes was tested. Fluorescence intensity of rhodamine 6G and fluorescein (dye concentration: 100ng/ml) with the existence of different concentrations of mercuric ion(from 1 ppb to 1000ppm) were measured. Mercuric ion shows a obvious quenching effect on Fluorescein but only little effect on Rhodamine 6G especially when the concentration of mercuric ion was in ppm range (See Figure 4-5).

Dye Release Experiment of DNA Capped MSN-R6G

In order to monitoring the dye release from the DNA capped MSN-R6G with the existence of mercuric Ions, 0.5 mg of DNA capped MSN-R6G was suspended in mercuric acetate binding buffer solution of different concentration(0ppb 10ppb 20ppb 50ppb 100ppb 200ppb 500ppb 1ppm, or the complimentary-Linker-DNA). As shown in Figure 4-6, the particle was suspended in 200μl mercuric solution in a Mini Dialysis Filter(Thermo Scientific, cut off molecular weight 7000) with a small piece of foam floating on the surface of 5ml mercuric solution in a 10ml beaker. The solution was kept stirring with a magnetic stir at 400rpm under room temperature and 150μl of solution was taken from the beaker to measure the fluorescence intensity with fluorescence spectrometer(HORIBA JobinYvon) every five minutes.

Results and Discussions

In our design, the Hg^{2+} was acting as the “key” to open the “door” of the dye released system and the detection signal was detected by measuring the fluorescence

intensity of released dye, which likes signal amplification process. The detailed paradigm is shown in Figure 4-7. The solid MSN was surface modified with isocyanate functional groups(MSN-NCO). After while this functionalization MSN-NCO was loaded with dye(Rhodamine 6G). We chose Rhodamine 6G as it had a relatively low quenching effect comparing with the other organic dyes(results shown in experimental section) And then dye loaded particle was obtain the dye doped MSN(MSN-R6G). Arm-DNA with the amino end(3'-NH2-AAA AAC AAC AAG AAG-5') was added on to the surface ofMSN-R6G by the chemical bind of –NCO and –NH2 group. After washed away the suspend Arm-DNA, a certain amount of T base rich Linker-DNA (5'-GTT GTT CTT CCT TTG TTT CCC CTT TCT TTG GTT GTT CTT C-3') was introduced to hybridize with the Arm-DNA. The single strand DNA was flexible and soft with a cross-sectional diameter of 0.6nm, which display a poor coverage of the pores on MSN[8,24]. After the addition of the Linker-DNA, the Linker-DNA would sonly hybridized with the Arm-DNA. As shown in Figure 4-8 one Linker-DNA had two binding sites with the Arm-DNA, we expect it cross-link with the Arm-DNA on the MSN surface, then form the more straight double-strand structure that significantly inhibit dye release by closing the pores. But only in the existence of Hg^{2+}, T-rich linker DNA would prefer to form intermolecular duplex then leave the MSN to release the dye molecule.

Fluorescence Test of Free DNA

In order to confirm that the Hg^{2+} can efficiently break the Linker-Arm DNA hybridization to form the new Linker-DNA intermolecule T-Hg-T duplex, we did the fluorescence test of the free DNA strands without particle in solution first. We designed a similar fluorophore-Linker-DNA but coupled fluorophore and quencher on each end(5'-FAM-GTT GTT CTT CCT TTG TTT CCC CTT TCT TTG GTT GTT CTT C Debcyl-

3')(Shown in Figure 4-9). While this DNA was in the "open" state, cause the distance between each end no fluorescence resonance energy transfer (FRET) would happen between the fluorophore and the quencher so the fluorescence signal could be detected. Only when this DNA was in the duplex state, for example, when the Hg^{2+} bond with the T bases to form a intermolecular T-Hg-T duplex, the fluorophore and quencher would be brought together then quench the fluorescence signal was quenched. Result as shown in Figure 4-10, fluorephore-Linker-DNA itself shown a strong fluorescence .Firstly we used excess amount of free Arm-DNA to hybridized with fluorephore-Linker-DNA first, then fluorephore-Linker-DNA was still in the "open" state without any FRET so fluorescence intensity was still strong. The small reduce of intensity was due to the quenching effect of duplex DNA on fluorophore. After while we titrated this solution with Hg^{2+} and a significant fluorescence reduction was been detected, which mean Hg^{2+} could efficiently dehybridize the Linker-Arm duplex and form the new T-Hg-T duplex. Then the excess amount of complimentary DNA to the Linker-DNA (cLinker-DNA 5'- GAA GAA CAA CCA AAG AAA GGG GAA ACA AAG GAA GAA CAA C -3') was introduced to the solution. We expected to see if this T-Hg-T duplex was strong enough to inhibit the hybridization between the fluorephore-Linker-DNA and cLinker-DNA. If the complimentary-Linker-DNA could open this T-Hg-T duplex then hybridize with it, then the fluorescence intensity should increase. But from the result only a small increase of fluorescence intensity was detected after the addition of complimentary-Linker-DNA . From this result it was confirmed that this intermolecular T-Hg-T duplex was very stable, even the complimentary DNA cannot open it. This result

confirmed that Hg^{2+} could be efficiently dehybridized the Linker-DNA from Arm-DNA then released the dye to express the fluorescence signal.

Detection of Hg^{2+} using Stimuli-Release Mesoporous System

In order to test the ability of this stimuli-release mesoporous system on the detection of Hg^{2+}, the dye release curve of MSN was been monitored under fluorescence spectrometer .We prepared 8 groups in each 0.5mg Linker-DNA capped MSN-R6G and then dispersed in mercuric acetate solution of different concentrations (0ppb 10ppb 20ppb 50ppb 100ppb 200ppb 500ppb 1ppm). Also we prepared the 9^{th} group of adding complimentary DNA (cLinker-DNA 5'- GAA GAA CAA CCA AAG AAA GGG GAA ACA AAG GAA GAA CAA C -3') to test the maximum opening of these system. The experimental process was described before. As can be seen in Figure 4-11, without Hg^{2+} a negligible release of Rhodamine 6G was tested, confirmed MSN-R6G was tightly capped by Linker-DNA (Brown curve in Figure 4-11). In the presence of Hg^{2+}, the DNA capped MSN-R6G was uncapped, the release of the Rhodamine 6G was detected and this release increase with the increase of the Hg^{2+} concentration . This system also gave a fast response to stimuli. Figure 4-12 shows the fluorescence signal after 20mins' release, and a significant increase of fluorescence intensity was detected in the solution with the increase of Hg^{2+} concentration, also this detectable limitation of the mercuric ion concentration can be down to 10ppb. The good limitation and the fast response suggested this method can be a fast and sensitive process for the detection of the Hg^{2+}.

Selectivity Test

To avoid the potential interference by other metal ions, the selectivity of this approach was tested. The dye release of Linker-DNA capped MSN-R6G particle was

also tested in the 1ppm solution of Lead(II) Acetate($PbAc_2$), Barium(II) Acetate($BaAc_2$), Iron(II) Acetate ($FeAc_2$), Iron(III) Chloride ($FeCl_3$), Zinc(II) Acetate($ZnAc_2$), Magnesium Acetate($MgAc_2$), Cadmium(II) Acetate($CdAc_2$), Copper(II) Acetate($CuAc_2$), Cobalt(II) Acetate ($CoAc_2$), Nickel(II) Acetate($NiAc_2$), Calcium(II) Acetate($CaAc_2$). The dye release process was measured as the same process as described before. The fluorescence intensities of solution after 20mins' release ware measured and normalized to the control groups(free dye release in buffer solution). Figure 4-13 shows that, in this specific stimuli-responsive dye release system , only the 1ppm Hg^{2+} solutions shown a 6.4 times fluorescence intensity to the control group, no interference from other metal ions was detected.

Conclusion

In this project, we developed a new DNA functionalized mesoporous silica nanoparticle dye release system to realize the direct, rapid, simple and sensitive detection of mercuric ion in aqueous system. This design was a combination of both DNA sensor technique and mesoporous material. Mosoporous silica nanoparticle was used as a container of dye and with the unique porous structure DNA sequences with specific length could be used for the capping of the pore. The long T-rich Linker-DNA was used to cap the pore while only with the existence of Hg^{2+}, the Linker-DNA will form the more stable T-Hg-T duplex with Hg^{2+} to uncap the pore and leave MSN. Only a small amount of "key" molecule could lead to the "door" open and released a large amount of cargo molecule through this signal amplification process. Fluorescence test results shows that this design can was rapid (less than 20min) and sensitive (ppb level) response to Hg^{2+} in aqueous solution. And due to the specific binding between T-rich DNA and $Hg^{2+,}$ this approach shown good selectivity and no potential interference by

other metal ions was detected. Comparing to other device-dependent ion detection techniques [58], this approach has no need for sample preparation, low cost in instruments, ease to operate, and the sensor particle is very stable under room condition, we strongly believe this approach would show great potential in developing new metal-ion sensing system for the detection of aqueous contamination.

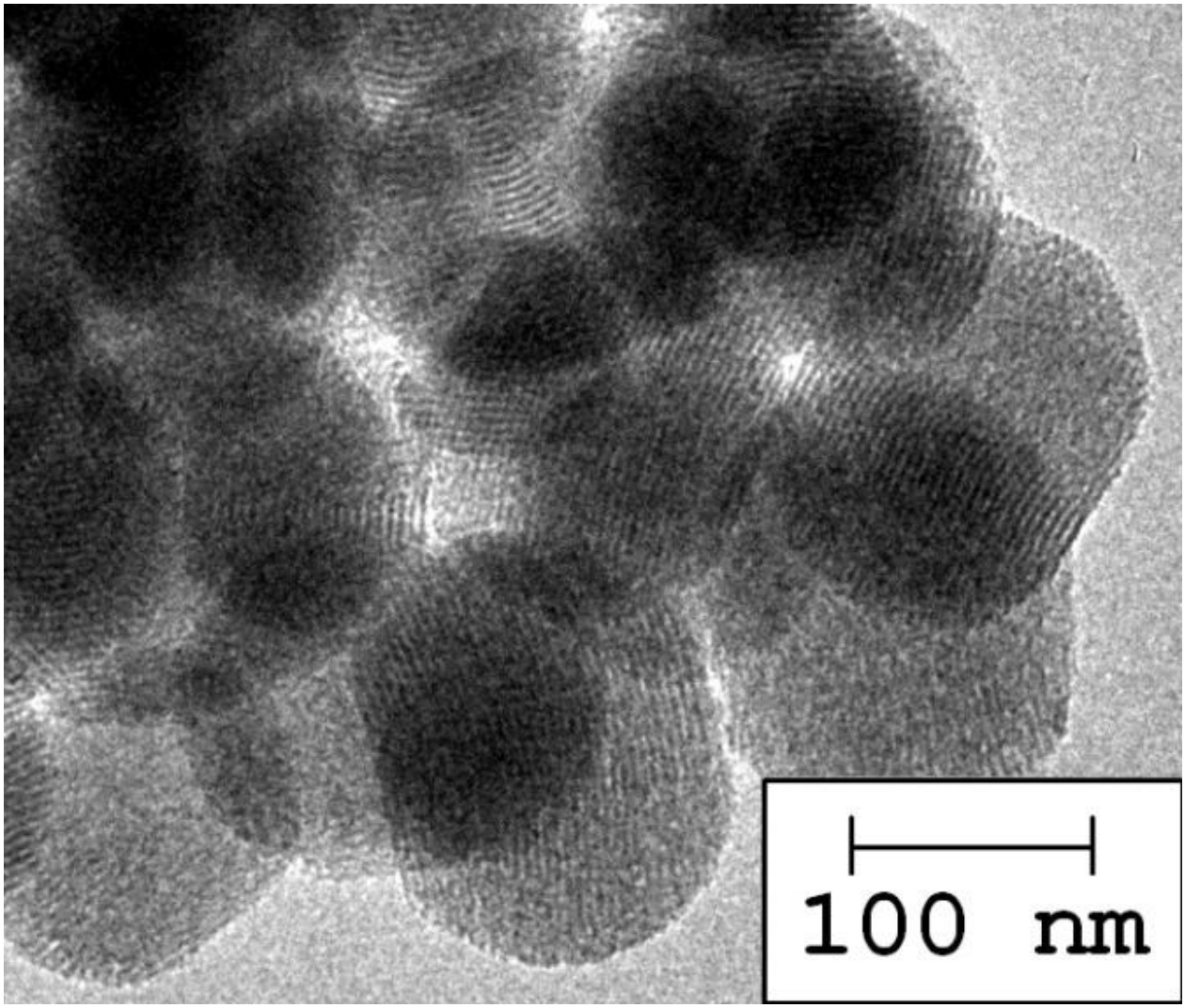

Figure 4-1. TEM image of mesoporous silica nanoparticle.

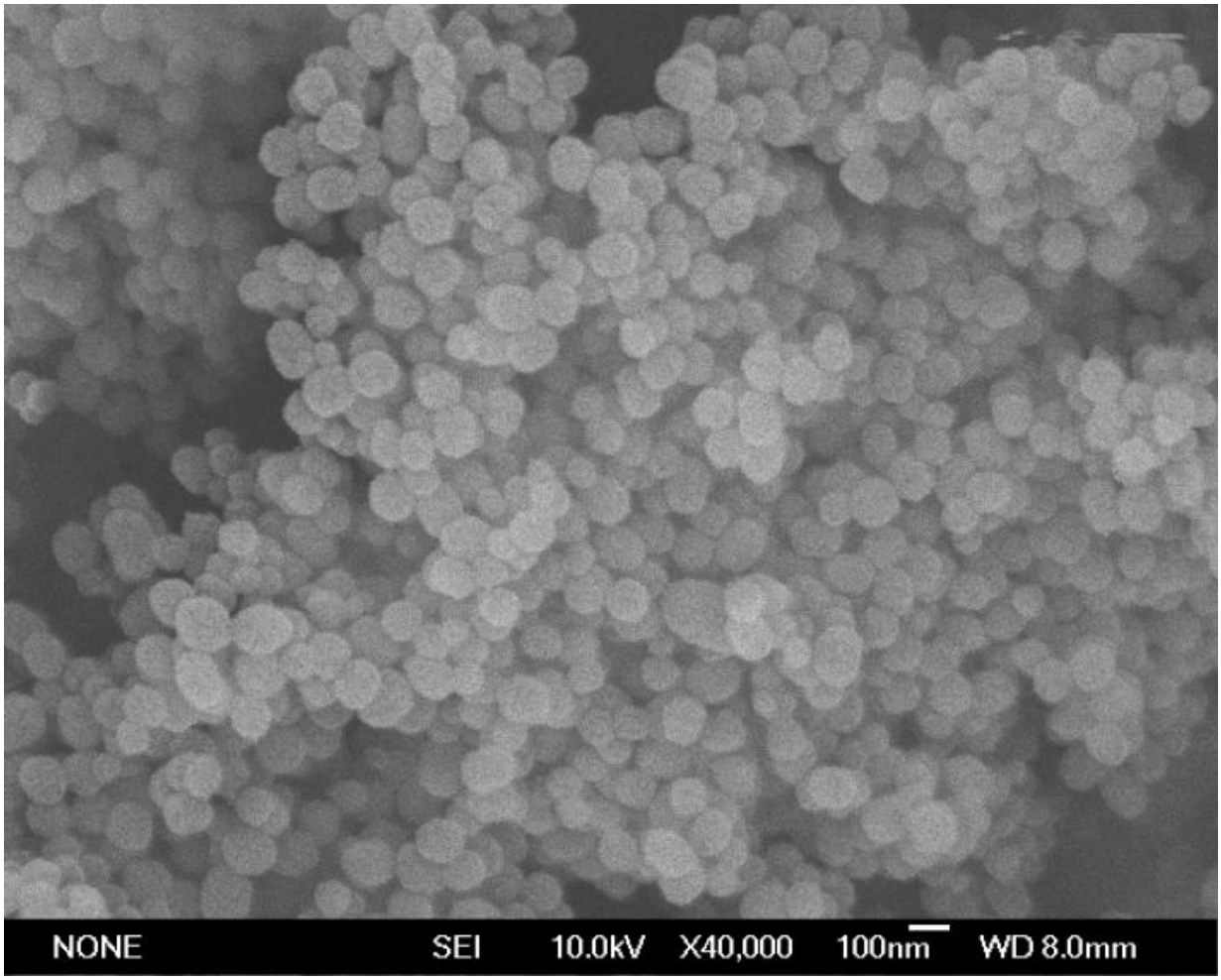

Figure 4-2. SEM image of mesoporous silica nanoparticle.

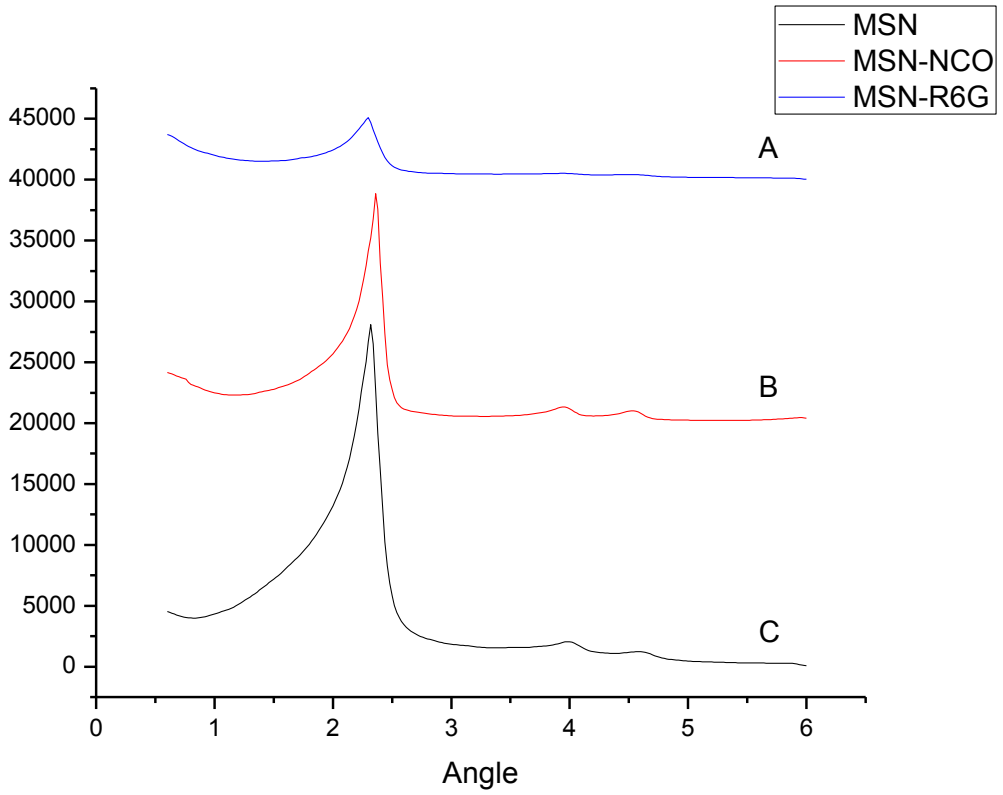

Figure 4-3. Powder X-ray patterns of the solids. A) mesoporous silica nanoparticle as synthesized and calcined. B) isocyanate group functionalized mesoporous silica nanoparticle. C) rhodamine 6G doped mesoporous silica nanoparticle.

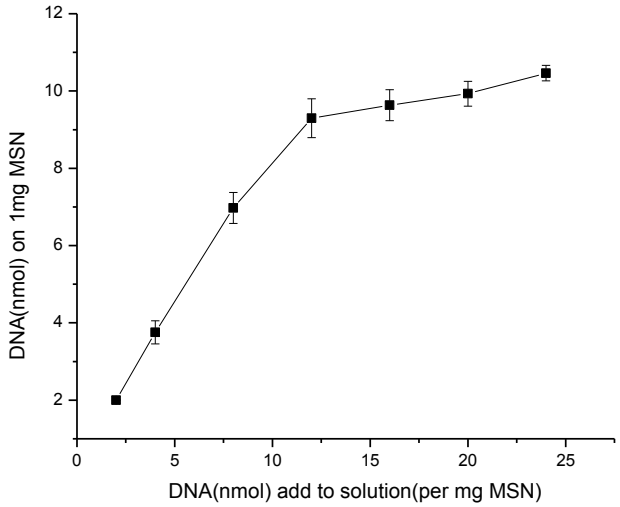

Figure 4-4. The titration curve of Arm-DNA binding on per gram of dye loaded mesoporous silica nanoparticle.

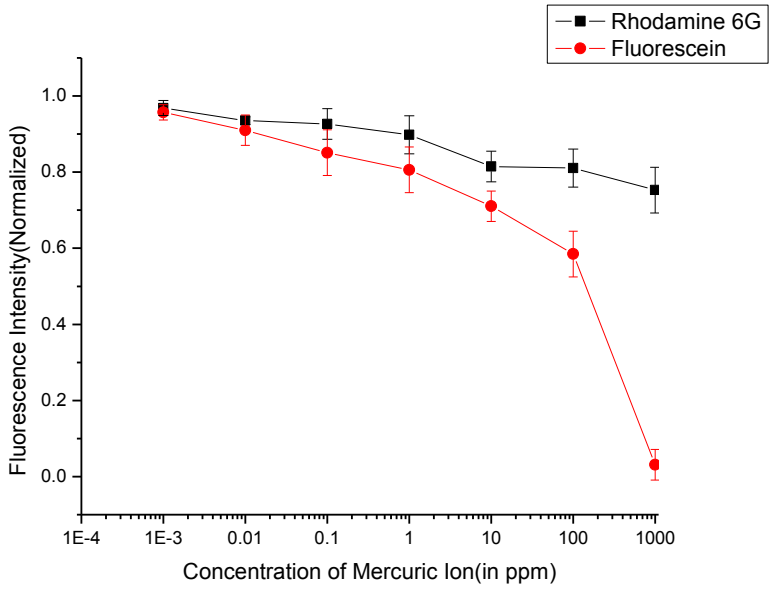

Figure 4-5. Quenching effect of mercuric ion on different organic dyes.

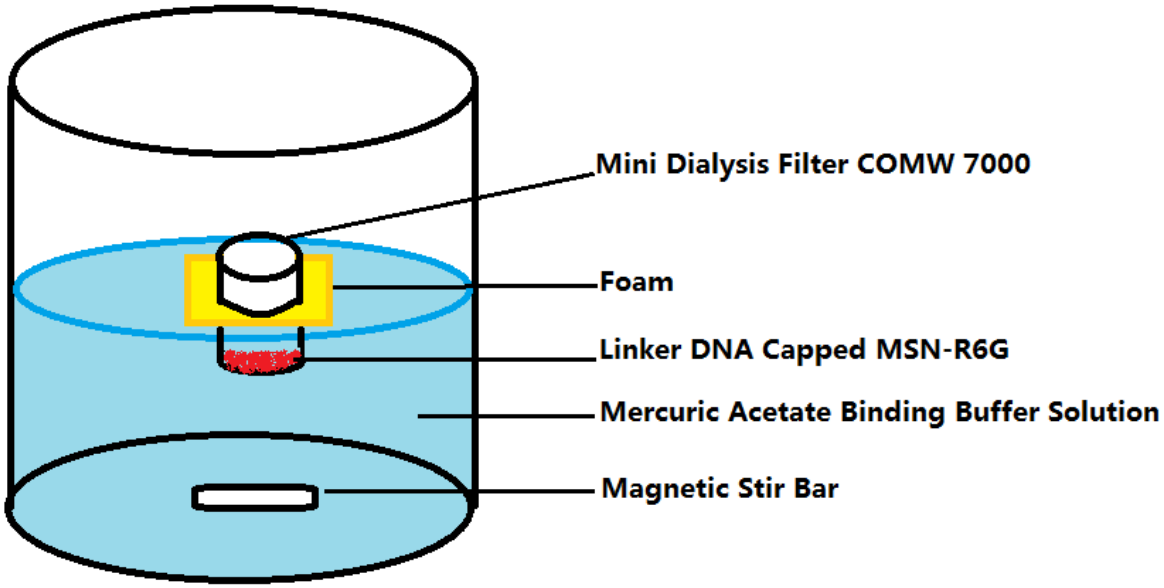

Figure 4-6. Setup of the mesoporous dye release device.

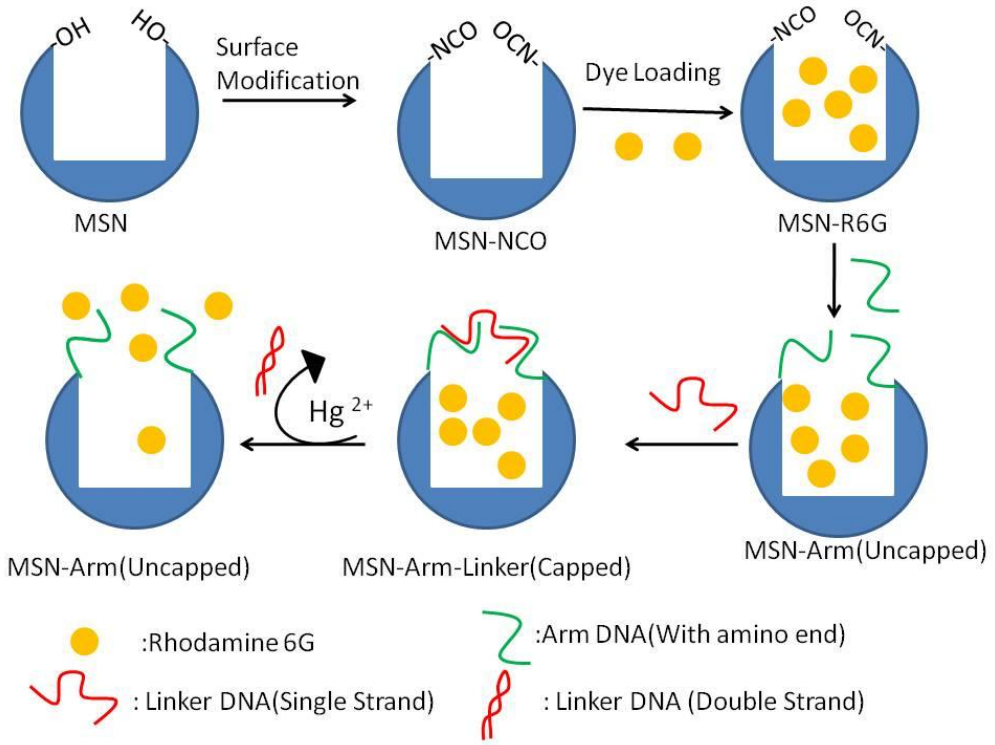

Figure 4-7. Schematic representation of the synthesis, surface modification, dye loading, DNA binding of the MSN and the dye release of the MSN in the existence of the Hg^{2+} .

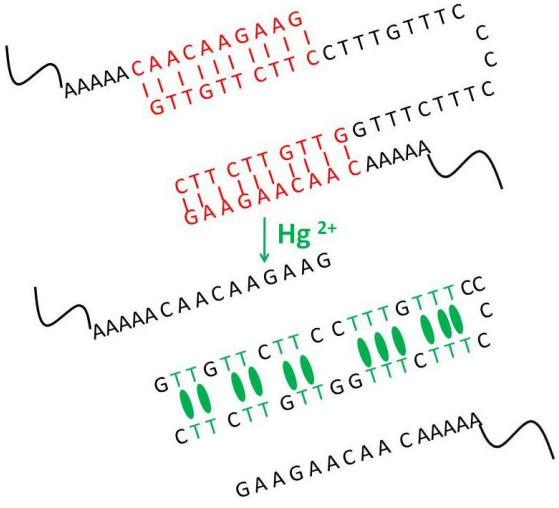

Figure 4-8. Hybridization of the Arm-DNA and Linker-DNA in the existence of Hg^{2+}.

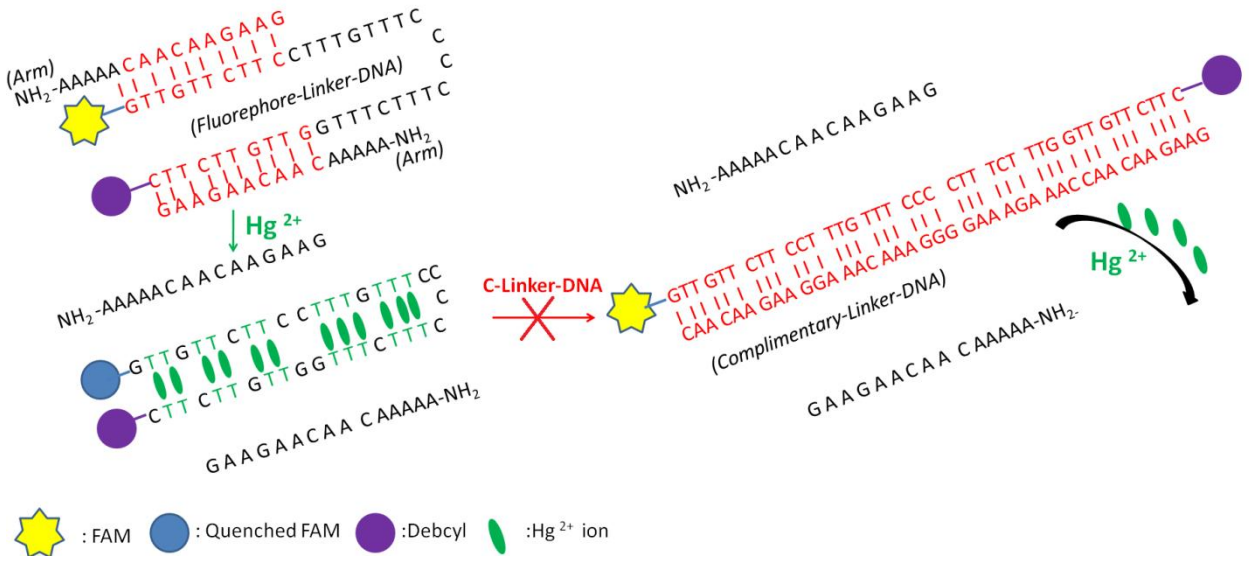

Figure 4-9. The scheme of the hybridization of the Arm-DNA, Fluorophore-Linker-DNA and Complimentary-Linker-DNA.

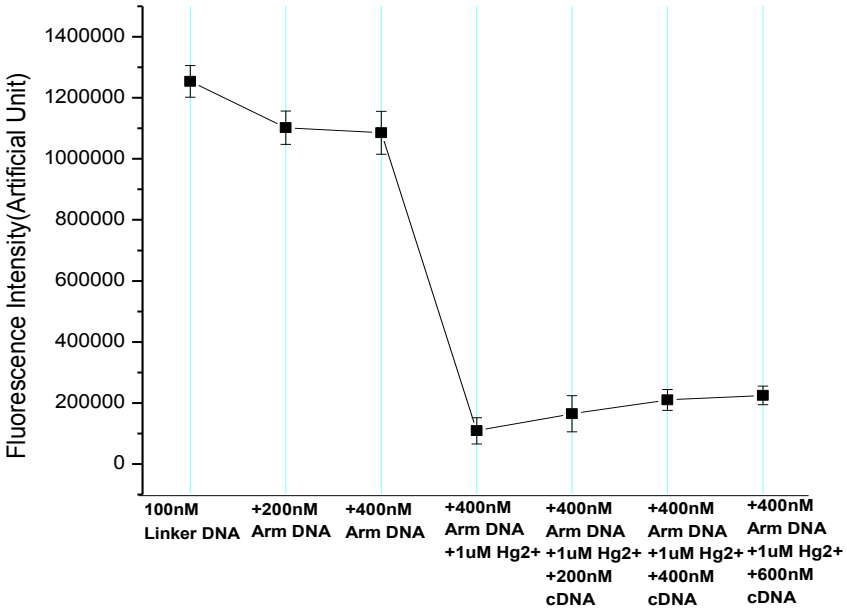

Figure 4-10. Fluorescence intensity of the 100nm Fluorophore-Linker-DNA solution after the addition of certain amount of Arm-DNA, Hg^{2+} and Complimentary-Linker-DNA.

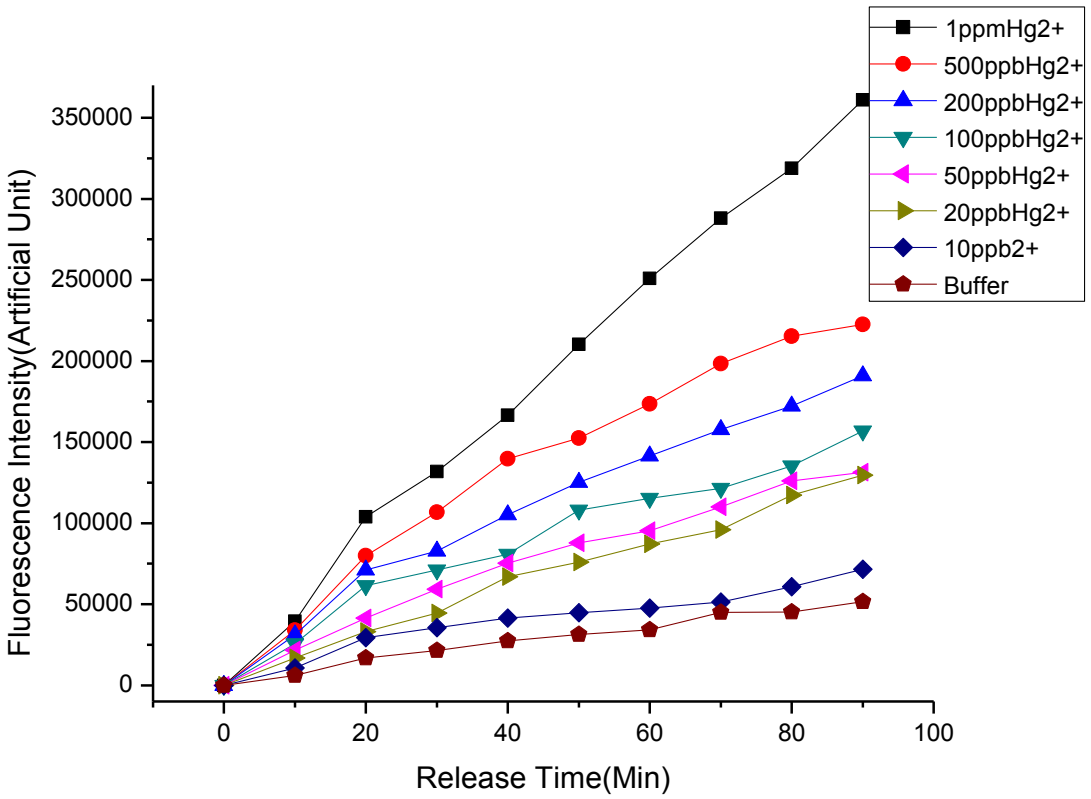

Figure 4-11. Release curve of rhodamine 6G from Linker-DNA capped MSN-R6G in mercuric acetate solution of different concentration. Laser excitation wavelength: 520nm.

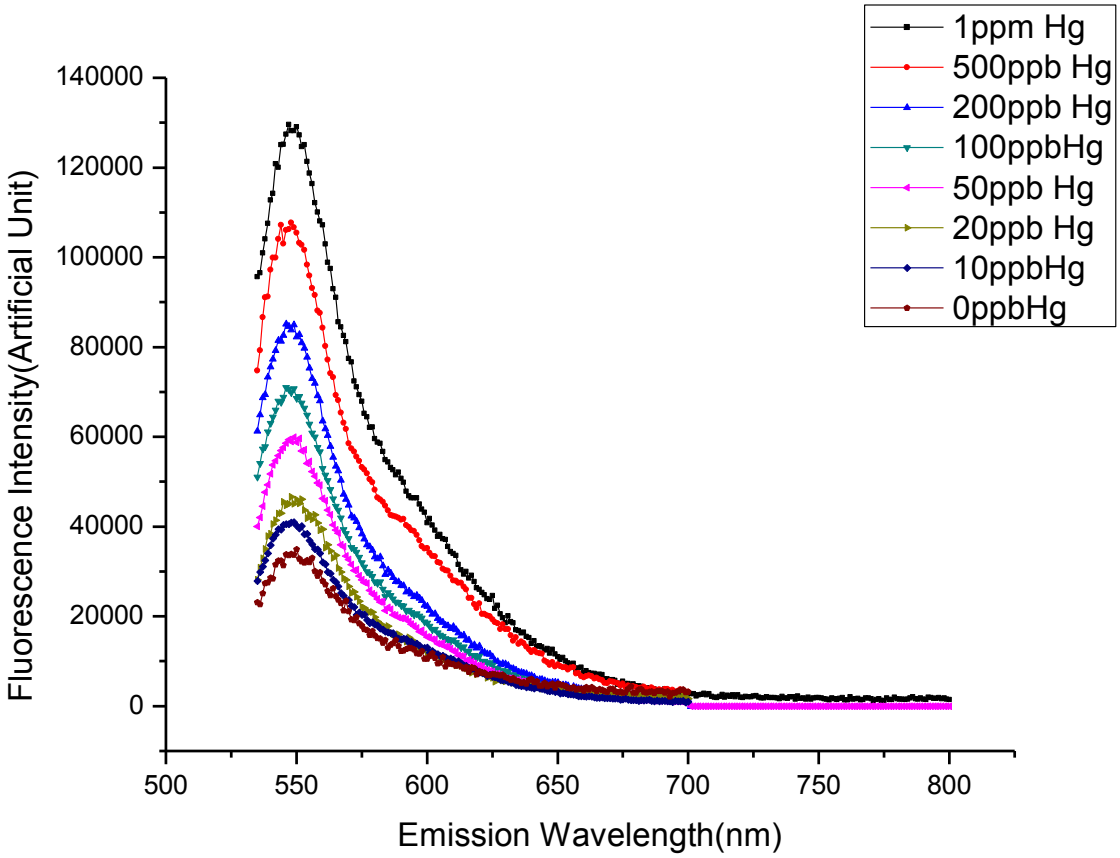

Figure 4-12. Fluorescence signal detected after 20 mins' release in mercuric acetate solution of different concentrations. Laser excitation wavelength: 520nm.

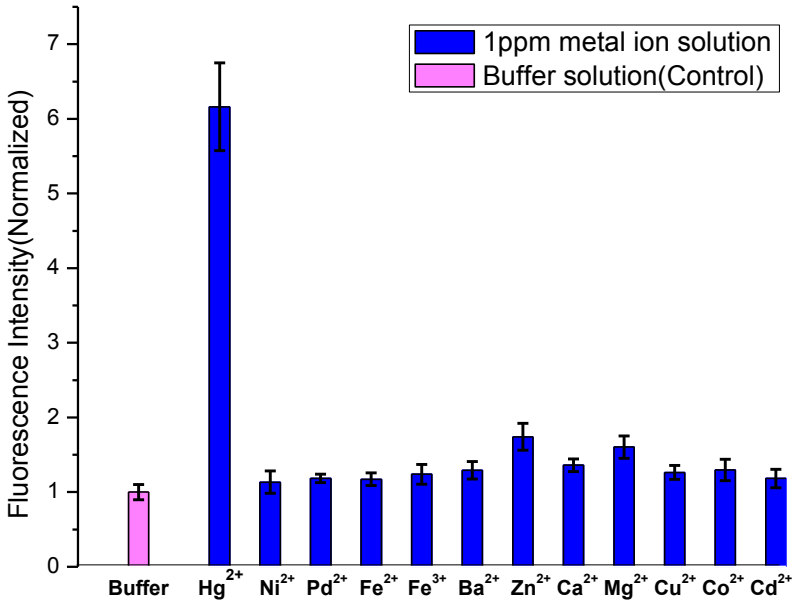

Figure 4-13. Fluorescence intensities of the released dye from Linker-DNA capped MSN-R6G in the presence of 1ppm different cation. The fluorescence intensities were normalized to the control. Release time: 20mins.

Table4-1. Sequence of Arm-DNA, Linker-DNA, and Fluorefore-Linker-DNA and Complimentary-Linker-DNA.

Sequence Name	Sequence
Arm-DNA	5’-GAA GAA CAA CAA AAA-NH_2-3’
Linker-DNA	5’-GTT GTT CTT CCT TTG TTT CCC CTT TCT TTG GTT GTT CTT C-3’
Fluorefore-Linker-DNA	5’-FAM-GTT GTT CTT CCT TTG TTT CCC CTT TCT TTG GTT GTT CTT C-Debcyl-3’
Complimentary-Linker-DNA	5’-G AAG AAC AAC CAA AGA AAG GGG AAA CAA AGG AAG AAC AAC-3’

CHAPTER 5
SUMMARY AND FUTURE DIRECTIONS

Incorporating Stimuli-responsive DNA Strands with Functional Nanomaterial for Biophysical and Analytical Applications

Stimuli-responsive DNA strands, with their sensitive and selectively response, have shown great potentials in molecular motor design, sensor design and drug delivery system development. With the help of functionalized nanoparticles, DNA technology can be developed to fulfill different applications, in both analytical and biophysical areas. All the three projects have one similarity: the combination of DNA and nanotechnology. Whereas DNA always acted as a sensitive probe, nanoparticles contributed from their special properties like metal particle's surface plasmons and mesoporous silica nanoparticle's hollow structure. In the first project, DNA was a light-driven nanomotor and silver nanoparticle was an "antenna" to convert irradiation energy into localized electric field. In the second project, DNA was a light-controlled "door" and mesoporous silica nanoparticle was a carrier of guest molecule. In the third project, DNA was an ion-responsive "door" and the silica particle was a dye container. With the esisting of numerous stimuli-responsive DNA strands and functional nanoparticles, it can be envisioned that a huge space of interdisciplinary between these two techniques has not been explored so far. The successful outcomes from these studies may lead to the advanced DNA nanoparticle hybridization in the analytical, biophysical, or even biomedical areas.

Future Directions

One future direction of DNA functionalized nanomaterials will serve as tools for target-specific drug delivery and release system. In particular, solving the serious side-effect caused by commercial available drugs in the anti-cancer study, a specific drug delivery system is highly demanding. This system should fulfill the requirements of (1) specific delivery of the drug to the tumor (2)selectively release of the drug around tumor cells (3) a mild release progress to avoid the overdose in human's body (4) stability and biocompatibility.

Considering these requirement I have designed an aptamer-capped target-responsive drug delivery and release system. Aptamers are single-stranded DNA or RNA oligonucleotides that with the specific recognition to a wide range of target molecules, from simple molecules to peptides, proteins and even living cells[59]. The anti-cancer drug doped mesoporous nanoparticles can be designed to be encapsulated by aptamer with high binding affinity to specific cancer cells(such as Sgc8 aptamer to CEM cell or TDO5 aptamer to RAMOS cell) After aptamer binding to cancer cell surface pores on mesoporous silica nanoparticles will be opened and anti-cancer drugs will be released accoradingly. Both aptamer and mesoporous silica nanoparticles are stable and biocompatible. We therefore expect this design can achieve the directly and targeted drug delivery toward tumor cells and reduce side-effect in cancer chemotherapy.

LIST OF REFERENCES

1 Campolongo, M. J. *et al.* Adaptive DNA-based materials for switching, sensing, and logic devices. *Journal of Materials Chemistry* **21**, 6113-6121 (2011).

2 Dahm, R. Discovering DNA: Friedrich Miescher and the early years of nucleic acid research. *Human genetics* **122**, 565-581 (2008).

3 Watson, J. D. & Crick, F. H. C. Molecular Structure of Nucleic Aicds- a Structure for Deoxyribose Nucleic Acid. *Nature* **171**, 737-738 (1953).

4 Chargaff, E., Zamenhof, S. & Green, C. Composition of human desoxypentose nucleic acid. *Nature* **165**, 756-757 (1950).

5 Gehring, K., Leroy, J. & Guéron, M. A tetrameric DNA structure with protonated cytosine-cytosine base pairs. *Nature* **363**, 561-565 (1993).

6 Liu , D. & Balasubramanian, S. A Proton-Fuelled DNA Nanomachine. *Angew. Chem. Int. Ed.* **42**, 5734-5736 (2003).

7 Shu, W. *et al.* DNA Molecular Motor Driven Micromechanical Cantilever Arrays. *Angew. Chem. Int. Ed.* **127**, 17054-17020 (2005).

8 Chen, C. *et al.* Stimuli-responsive controlled-release system using quadruplex DNA-capped silica nanocontainers. *Nucleic Acids Research* **39**, 1638-1644 (2011).

9 Surana, S., Bhat, J. M., Koushika, S. P. & Krishnan, Y. An autonomous DNA nanomachine maps spatiotemporal pH changes in a multicellular living organism. *Nature Communications* **2** 340 (2011).

10 Asanuma, H. *et al.* Synthesis of azobenzene-tethered DNA for reversible photoregulation of DNA functions: hybridization and transcription. *Nature Protocols*, **2** 203-212 (2007).

11 Bai, X., Li, Z., Jockusch, S., Turro, N. J. & Ju, J. Photocleavage of a 2-nitrobenzyl linker bridging a fluorophore to the 5' end of DNA. *Proceedings of National Academy of Sciences of the United States of America* **100**, 409-413 (2003).

12 Kang, H. *et al.* Single-DNA Molecule Nanomotor Regulated by Photons. *Nano Letters* **9**, 2690-2696 (2009).

13 Han, D. *et al.* Molecular engineering of photoresponsive three-dimensional DNA nanostructures. *chemical Communications* **47**, 4670-4672 (2011).

14 Lee, J., Han, M. S. & Mirkin, C. A. Colorimetric Detection of Mercuric Ion (Hg2+) in Aqueous Media using DNA-Functionalized Gold Nanoparticles. *Angewandte Chemie International Edition* **46**, 4093-4096 (2007).

15 Neeshma Dave, M. Y. C., Po-Jung Jimmy Huang, Brendan D. Smith, Juewen Liu. Regenerable DNA-Functionalized Hydrogels for Ultrasensitive, Instrument-Free Mercury(II) Detection and Removal in Water. *J. Am. Chem. Soc.* **132**, 12668–12673 (2010).

16 Mie, G. Beiträge zur Optik trüber Medien, speziell kolloidaler Metallösungen. *Annalen Der Physik* **330**, 377-455 (1908).

17 Tan, S. J., Campolongo, M. J., Luo, D. & Cheng, W. Building plasmonic nanostructures with DNA. *Nature Nanotechnology* **6**, 268-276 (2011).

18 Wang, H., Brandl, D. W., Nordlander, P. & Halas, N. J. Plasmonic Nanostructures: Artificial Molecules. *Accounts of Chemical Research* **40**, 53-62 (2007).

19 Mulvaney, P. Surface Plasmon Spectroscopy of Nanosized Metal Particles. *Langmuir* **12**, 788-800 (1996).

20 Kelly, K. L., Coronado, E., Zhao, L. L. & Schatz, G. C. The Optical Properties of Metal Nanoparticles: The Influence of Size, Shape, and Dielectric Environment. *The Journal of Physical Chemistry B* **107**, 668-677 (2003).

21 Liz-Marzán, L. M. Tailoring Surface Plasmons through the Morphology and Assembly of Metal Nanoparticles. *Langmuir* **22**, 32-41 (2006).

22 Beck, J. S. *et al.* A new family of mesoporous molecular sieves prepared with liquid crystal templates. *Journal of American Chemical Society* **114**, 10834-10843 (1992).

23 Zhao, D. *et al.* Triblock Copolymer Syntheses of Mesoporous Silica with Periodic 50 to 300 Angstrom Pores. *Science* **279**, 548-552 (1998).

24 Lee, C. *et al.* Intracellular pH-Responsive Mesoporous Silica Nanoparticles for the Controlled Release of Anticancer Chemotherapeutics. *Angew. Chem. Int. Ed.* **49**, 8214-8219 (2010).

25 Climent, E. *et al.* Controlled Delivery Using Oligonucleotide-Capped Mesoporous Silica Nanoparticles. *Angew. Chem. Int. Ed.* **49**, 7281-7283 (2010).

26 Schlossbauer, A. *et al.* A Programmable DNA-Based Molecular Valve for Colloidal Mesoporous Silica. *Angew. Chem. Int. Ed.* **49**, 4734-4737 (2010).

27 Schlossbauer, A., Kecht, J. & Bein, T. Biotin–Avidin as a Protease-Responsive Cap System for Controlled Guest Release from Colloidal Mesoporous Silica. *Angewandte Chemie* **121**, 3138-3141 (2009).

28 Zhu, C., Lu, C., Song, X., Yang, H. & Wang, X. Bioresponsive Controlled Release Using Mesoporous Silica Nanoparticles Capped with Aptamer-Based Molecular Gate. *J. Am. Chem. Soc.* **133**, 1278-1281 (2011).

29 Liu, R. *et al.* pH-Responsive Nanogated Ensemble Based on Gold-Capped Mesoporous Silica through an Acid-Labile Acetal Linker. *J. Am. Chem. Soc.* **132**, 1500-1501 (2010).

30 Thomas, C. R. *et al.* Noninvasive Remote-Controlled Release of Drug Molecules in Vitro Using Magnetic Actuation of Mechanized Nanoparticles. *J. Am. Chem. Soc.* **132**, 10623-10625 (2010).

31 Patel, K. *et al.* Enzyme-Responsive Snap-Top Covered Silica Nanocontainers. **130**, 2382-2383 (2008).

32 Park, C., Lee, K. & Kim, C. Photoresponsive Cyclodextrin-Covered Nanocontainers and Their Sol-Gel Transition Induced by Molecular Recognition. *Angew. Chem. Int. Ed.* **48**, 1275-1278 (2009).

33 Park, C., Kim, H., Kim, S. & Kim, C. Enzyme Responsive Nanocontainers with Cyclodextrin Gatekeepers and Synergistic Effects in Release of Guests. *J. Am. Chem. Soc.* **131**, 16614-16615 (2009).

34 Zhao, Y., Trewyn, B. G., Slowing, I. I. & Lin, S. Y. Mesoporous Silica Nanoparticle-Based Double Drug Delivery System for Glucose-Responsive Controlled Release of Insulin and Cyclic AMP. **131**, 8398-8400 (2009).

35 Bernardos, A. *et al.* Enzyme-Responsive Controlled Release Using Mesoporous Silica Supports Capped with Lactose. *Angewandte Chemie* **121**, 5598-6001 (2009).

36 Yurke, B., Turberfield, A. J., Mills, A. P., Simmel, F. C. & Neumann, J. L. A DNA-fuelled molecular machine made of DNA. *Nature* **406**, 605-608 (2000).

37 Yan, H., Zhang, X., Shen, Z. & N.C., S. A robust DNA mechanical device controlled by hybridization topology. *Nature* **415**, 62-65 (2002).

38 Shin, J. & Pierce, N. A. A Synthetic DNA Walker for Molecular Transport. *Journal of American Chemical Society* **126**, 10834-10835 (2004).

39 Modi, S. *et al.* A DNA nanomachine that maps spatial and temporal pH changes inside living cells. *Nature Nanotechnology* **4**, 325-330 (2009).

40 Sun, Y., Gates, B., Mayers, B. & Xia, Y. Crystalline Silver Nanowires by Soft Solution Processing. *Nano Letters* **2**, 165-168 (2002).

41 Johnson, P. B. & Christy, R. W. Optical Constants of the Noble Metals. *Physical Review B* **6**, 4370-4379 (1972).

42 Ahonen, P., Schiffrin, D. J., Paprotny, J. & Kontturi, K. Optical switching of coupled plasmons of Ag-nanoparticles by photoisomerisation of an azobenzene ligand *Physical Chemistry Chemical Physics* **9**, 651-658 (2007).

43 Manna, A. *et al.* Optimized Photoisomerization on Gold Nanoparticles Capped by Unsymmetrical Azobenzene Disulfides. *Chemistry of Materials* **15**, 20-28 (2003).

44 Du, C., You, Y., Zhang, X., Johnson, K. & Shen, Z. Polarization-Dependent Confocal Imaging of Individual Ag Nanorods and Nanoparticles. *Plasmonics* **4**, 217-222 (2009).

45 Ni, W., Yang, Z., Chen, H., Li, L. & Wang, J. Coupling between Molecular and Plasmonic Resonances in Freestanding Dye−Gold Nanorod Hybrid Nanostructures. *Journal of American Chemical Society* **130**, 6692-6693 (2008).

46 Yuan, Q. *et al.* Using silver nanowire antennas to enhance the conversion efficiency of photoresponsive DNA nanomotors. *Proceedings of National Academy of Sciences of the United States of America* (2011).

47 Wang, H. *et al.* Engineering a Unimolecular DNA-Catalytic Probe for Single Lead Ion Monitoring. *Journal of American Chemical Society* **131**, 8221-8226 (2009).

48 Li, T., Dong, S. & Wang, E. Label-Free Colorimetric Detection of Aqueous Mercury Ion (Hg2+) Using Hg2+-Modulated G-Quadruplex-Based DNAzymes. *Analytical Chemistry* **81**, 2144-2149 (2009).

49 Elbaz, J., Wang, Z., Orbach, R. & Willner, I. pH-Stimulated Concurrent Mechanical Activation of Two DNA “Tweezers”. A “SET−RESET” Logic Gate System. *Nano Letters* **9**, 4510-4514 (2009).

50 Tao Li , S. D., Erkang Wang. Label-Free Colorimetric Detection of Aqueous Mercury Ion (Hg2+) Using Hg2+-Modulated G-Quadruplex-Based DNAzymes. *Analytical Chemistry* **81**, 2144-2149 (2009).

51 Dave, N., Chan, M., Huang, P., Smith, B. & Liu, J. Regenerable DNA-Functionalized Hydrogels for Ultrasensitive Instrument-Free Mercury(II) Detection and Removal in Water. *JACS* **132**, 12668-12673 (2010).

52 Mercury Update: Impact of Fish Advisories. EPA Fact Sheet EPA-823-F-01-011; EPA, Office of Water: Washington, DC, 2001.

53 Nolan, E. & Lippard, S. Tools and Tactics for the Optical Detection of Mercuric Ion. *Chemical Review* **108**, 3433-3480 (2008).

54 Chiang, C., Huang, C., Liu, C. & Chang, H. Oligonucleotide-Based Fluorescence Probe for Sensitive and Selective Detection of Mercury(II) in Aqueous Solution. *Analytical Chemistry* **80**, 3716-3721 (2008).

55 Lee, J. & Mirkin, C. A. Chip-Based Scanometric Detection of Mercuric Ion Using DNA-Functionalized Gold Nanoparticles. *Analytical Chemistry* **80**, 6805-6808 (2008).

56 Chen, P. & He, C. A General Strategy to Convert the MerR Family Proteins into Highly Sensitive and Selective Fluorescent Biosensors for Metal Ions. *J. Am. Chem. Soc.* **126**, 728-729 (2004).

57 Climent, E. *et al.* The Determination of Methylmercury in Real Samples Using Organically Capped Mesoporous Inorganic Materials Capable of Signal Amplification. *Angewandte Chemie International Edition* **48**, 8519-8522 (2009).

58 Chen, J., Chen, H., Jin, X. & Chen, H. Determination of ultra-trace amount methyl-, phenyl- and inorganic mercury in environmental and biological samples by liquid chromatography with inductively coupled plasma mass spectrometry after cloud point extraction preconcentration *Talanta* **77**, 1381-1387 (2009).

59 Zhang, Y., Chen, Y., Han, D., Ocsoy, I. & Tan, W. Aptamers selected by cell-systematic evolution of ligands by exponential enrichment for application in cancer studies. *Bioanalysis* **2**, 907-918 (2010).

BIOGRAPHICAL SKETCH

Yunfei Zhang was born in Hefei, Anhui Province, China, on 1990. In 2002 she entered the Hefei NO.1 High school scientific genius class as the only full score in Chemistry of Anhui Province. In 2005 Yunfei entered University of Science and Technology of China with major in Chemical Physics and entered Dr Lifeng Yan's lab to start her individual research on biomaterial extraction. After two-year work, Yunfei wrote a first-author paper that published on Chinese Polymer Bulletin, which also made her be awarded the "Outstanding Undergraduate Research Program" of USTC. In 2009 Yunfei came to US to continue her research under the guidance of Dr. Weihong Tan of University of Florida.